



OPEN HIF-1 regulates mitochondrial function in bone marrow-derived macrophages but not in tissue-resident alveolar macrophages

Parker S. Woods, Rengül Cetin-Atalay, Angelo Y. Meliton, Kaitlyn A. Sun, Obada R. Shamaa, Kun Woo D. Shin, Yufeng Tian, Benjamin Haugen, Robert B. Hamanaka & Gökhan M. Mutlu✉

HIF-1 α plays a critical role in shaping macrophage phenotype and effector function. We have previously shown that tissue-resident alveolar macrophages (TR-AMs) have extremely low glycolytic capacity at steady-state but can shift toward glycolysis under hypoxic conditions. Here, we generated mice with tamoxifen-inducible myeloid lineage cell specific deletion of *Hif1a* (*Hif1a^{fl/fl};LysM-CreERT2^{+/-}*) and from these mice, we isolated TR-AMs and bone marrow-derived macrophages (BMDMs) in which *Hif1a* is deleted. We show that TR-AM HIF-1 α is required for the glycolytic shift under prolyl hydroxylase inhibition but is dispensable at steady-state for inflammatory effector function. In contrast, HIF-1 α deletion in BMDMs led to diminished glycolytic capacity at steady-state and reduced inflammatory capacity, but higher mitochondrial function. Gene set enrichment analysis revealed enhanced c-Myc transcriptional activity in *Hif1a^{-/-}* BMDMs, and upregulation of gene pathways related to ribosomal biogenesis and cellular proliferation. We conclude that HIF-1 α regulates mitochondrial function in BMDMs but not in TR-AMs. The findings highlight the heterogeneity of HIF-1 α function in distinct macrophage populations and provide new insight into how HIF-1 α regulates gene expression, inflammation, and metabolism in different types of macrophages.

Keywords Alveolar macrophage, Bone marrow-derived macrophage, HIF-1 α , Metabolism, Mitochondria, Inflammation

It is well-established that glycolytic metabolism plays a central role in regulating immune cell effector function^{1–5}. As the field of immunometabolism grew, it has become more apparent that tissue-specific conditions lead to unique metabolic characteristics that often fall outside of the conventional framework ascribed to broader immune cell populations^{6–8}. For instance, while bone marrow-derived macrophages (BMDMs) rely predominantly on glycolysis for proinflammatory processes, we have found glycolysis to be dispensable for inflammation in tissue-resident alveolar macrophages (TR-AMs)⁹. It is likely that the unique environment of the alveolar lumen dictates the metabolic needs of TR-AMs¹⁰. Glucose concentrations within the airway are approximately one-tenth of those observed in the blood, and oxygen levels are the highest of any compartment within the human body making oxidative phosphorylation a more efficient means of metabolism for TR-AMs^{6,11}. While TR-AMs do not conduct glycolysis under steady-state conditions, they can be pushed toward a glycolytic phenotype under severe hypoxia such as in cases of acute respiratory distress syndrome (ARDS) where lung oxygenation is impaired¹². Further highlighting the role of the alveolar niche in dictating cellular phenotype, BMDMs, peritoneal macrophages, and macrophage precursors transplanted into the airway acquire phenotypical characteristics associated with TR-AM identity^{8,13}. Together, these findings show that TR-AMs reside in a unique environment that negates the need for glycolytic metabolism under steady-state conditions.

It is widely understood that the transcription factor hypoxia-inducible factor 1- α (HIF-1 α) is a key regulator of glycolysis, particularly at low oxygen concentrations¹⁴. Under normoxia, HIF-1 α is marked for proteasomal degradation by oxygen-dependent prolyl hydroxylases. In contrast, under hypoxia, prolyl hydroxylase activity is diminished so that HIF-1 α accumulates and can enter the nucleus to promote transcriptional adaptation to low oxygen levels. Much of the HIF-1 α transcriptional response relates to cell survival under oxygen depleted conditions, including upregulation of genes related to glycolysis, angiogenesis, and cell survival. In macrophages of monocytic origin, HIF-1 α functions outside the context of the hypoxic response. HIF-1 α has been shown to

Department of Medicine, Section of Pulmonary and Critical Care Medicine, The University of Chicago, 5841 S. Maryland Avenue MC6026, Chicago, IL 60637, USA. ✉email: gmutlu@uchicago.edu

be a key regulator of macrophage migration and proinflammatory processes^{15–18}. Both HIF-1 α and glycolysis are induced in BMDMs treated with lipopolysaccharide (LPS), but whether HIF-1 α is required for the observed glycolytic reprogramming or just for inflammatory processes remains unknown. Moreover, HIF-1 α behaves differently in TR-AMs^{12,19}. As we have shown, hypoxia induces HIF-1 α stabilization in TR-AMs, but not in BMDMs¹². HIF-1 α and its target genes are downregulated in TR-AMs following birth, and this downregulation is required for normal TR-AM maturation and function¹⁹. Thus, the full extent for how HIF-1 α regulates macrophage function remains unclear.

To gain a more complete understanding of how HIF-1 α regulates macrophage metabolism and effector function, we deleted HIF-1 α from both BMDMs and TR-AMs and performed metabolic and immunological assays. We found that deletion of HIF-1 α in mature TR-AMs had no effect on steady-state metabolic function or gene expression. Phenotypical alterations only became apparent in the presence of prolyl hydroxylase inhibitor FG-4592 where HIF-1 α knockout TR-AMs failed to take on a glycolytic phenotype and remained highly susceptible to cell death in the presence of electron transport chain (ETC) inhibitors. Conversely, HIF-1 α deletion in BMDMs greatly diminished their glycolytic capabilities at both steady-state and in the presence of FG-4592, sensitizing these cells to ETC inhibitor-induced cell death. HIF-1 α knockout BMDMs presented with higher mitochondrial oxygen consumption rates, tricarboxylic acid (TCA) cycle metabolite levels, and ETC gene and protein expression compared to controls. This was not the case with TR-AMs.

We found that neither HIF-1 α nor glycolysis was induced in TR-AMs upon LPS stimulation, and that TR-AMs with HIF-1 α knockout exhibited no observable alterations in TCA cycle metabolite levels or cytokine production. In contrast, deletion of HIF-1 α in BMDMs led to reductions in LPS-induced glycolysis, but the magnitude of the response did not differ substantially from control BMDMs. HIF-1 α knockout BMDMs also exhibited reductions in cytokine production but presented with higher TCA cycle metabolite levels following LPS treatment. Gene set enrichment analysis of HIF-1 α knockout BMDMs revealed the upregulation c-Myc-dependent transcriptional programs, including genes related to ribosomal biogenesis and cellular proliferation. Collectively, these findings highlight the heterogeneity of HIF-1 α function in distinct macrophage populations and provide new insight into how HIF-1 α regulates inflammation and metabolism in macrophages.

Results

HIF-1 α deletion alters transcriptome both at baseline and following treatment with a HIF-1 α stabilizer in BMDMs but only after HIF-1 α stabilizer in TR-AMs

We have recently demonstrated that TR-AMs have a very low glycolytic capacity at steady-state but can be pushed toward a glycolytic phenotype under hypoxic conditions¹². Whether this metabolic reprogramming depends on HIF-1 α is unknown. To study the role of HIF-1 α in metabolic reprogramming in TR-AMs, we generated mice with tamoxifen-inducible myeloid lineage cell specific deletion of *Hif1a* (*Hif1a*^{fl/fl}:*LysM-CreERT2*^{+/−}) by crossing *Hif1a*^{fl/fl} mice (B6.129-*Hif1a*^{tm3Rsjof}) (Jackson Strain #: 007561) with *LysM-CreERT2*^{+/−} mice (heterozygous for inducible Cre recombinase) (*Lyz2*^{tm1(cre/ERT2)Grtn/J}) (Jackson Strain #: 031674). Using these mice, we deleted HIF-1 α in TR-AMs and BMDMs (Fig. 1A, D) respectively. Successful deletion of HIF-1 α was confirmed by measurement of *Hif1a* exon 2 expression by qPCR (Supplementary Fig. S1). For simplicity, we will refer to TR-AMs and BMDM with inducible deletion of *Hif1a* as *Hif1a*^{−/−} cells. In control (*Hif1a*^{+/+}) TR-AMs and BMDMs, FG-4592 (a potent prolyl hydroxylase inhibitor, which stabilizes HIF-1 α protein) caused a similar induction of HIF-1 α expression (Supplementary Fig. S2). Deletion of *Hif1a* led to loss of FG-4592-induced stabilization of HIF-1 α protein as expected (Fig. 1A, D). To determine the role of HIF-1 α in transcriptional activity in TR-AMs and BMDMs, we performed RNA-sequencing. Both *Hif1a*^{+/+} and *Hif1a*^{−/−} macrophages were treated overnight with FG-4592 or left untreated. We found that loss of HIF-1 α in TR-AMs resulted in minimal changes in gene expression at baseline with only 10 observed significantly differentially expressed genes (DEGs, Log2 fold change ≥ 1 and $p \leq 0.05$) (8 upregulated and 2 downregulated) when compared to controls (Fig. 1B, Supplementary Fig. S3A). Treatment of control (*Hif1a*^{+/+}) TR-AMs with FG-4592 led to 953 DEGs (522 upregulated and 431 downregulated). Compared to control TR-AMs, the effect of FG-4592 was greatly diminished in *Hif1a*^{−/−} TR-AMs which exhibited 197 DEGs (157 upregulated and 40 downregulated). Heatmap analysis for HIF-1 α target genes confirmed that *Hif1a*^{−/−} TR-AMs exhibited a greatly diminished response to FG-4592 in a HIF-1 α specific manner (Fig. 1C).

In contrast to TR-AMs, HIF-1 α deletion resulted in significant alterations at baseline in BMDMs with 305 DEGs (121 upregulated and 184 downregulated). After FG-4592 treatment, only 126 DEGs (60 upregulated and 66 downregulated) were observed in *Hif1a*^{−/−} BMDMs compared to 694 DEGs (323 upregulated and 371 downregulated) in control BMDMs (Supplementary Fig. S3B). Heatmap analysis for HIF-1 α target genes further demonstrated that *Hif1a*^{−/−} BMDMs exhibit significant basal alterations in gene expression and a substantial reduction in their response to FG-4592 in a HIF1 α -specific manner (Fig. 1F).

Collectively, these data validate our previous findings documenting that HIF-1 α is dispensable in TR-AMs under steady-state conditions. These data also support the current literature pointing to HIF-1 α as a key regulator of normal BMDM transcriptional response and function.

HIF-1 α deletion broadly impairs glycolysis in BMDMs but only impairs TR-AM glycolysis following HIF-1 α stabilizer treatment

We next sought to assess the functional consequences of HIF-1 α deletion in our two macrophage populations by evaluating overall glycolytic fitness. To do so, we performed a glycolysis stress test and measured glycolysis, assessed by extracellular acidification rate (ECAR), after overnight (16 h) treatment with FG-4592. Loss of HIF-1 α did not affect baseline glycolytic rate in TR-AMs, as *Hif1a*^{−/−} TR-AMs did not exhibit any changes in their glycolytic rate compared to control TR-AMs, which already had low glycolysis (Fig. 2A and B). As expected, FG-4592 induced an increase in glycolytic rate in control *Hif1a*^{+/+} TR-AMs (Fig. 2A and B). However,

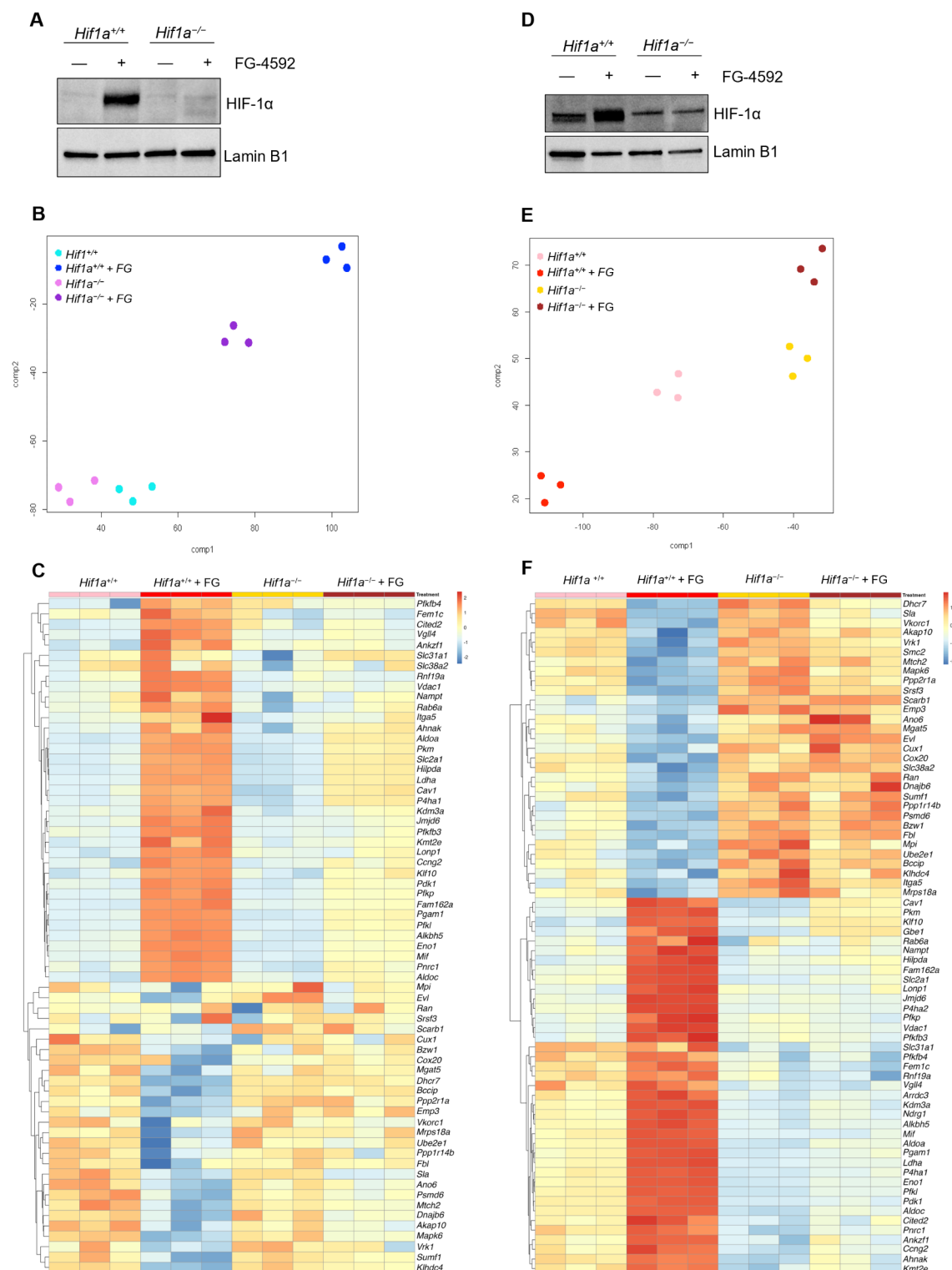
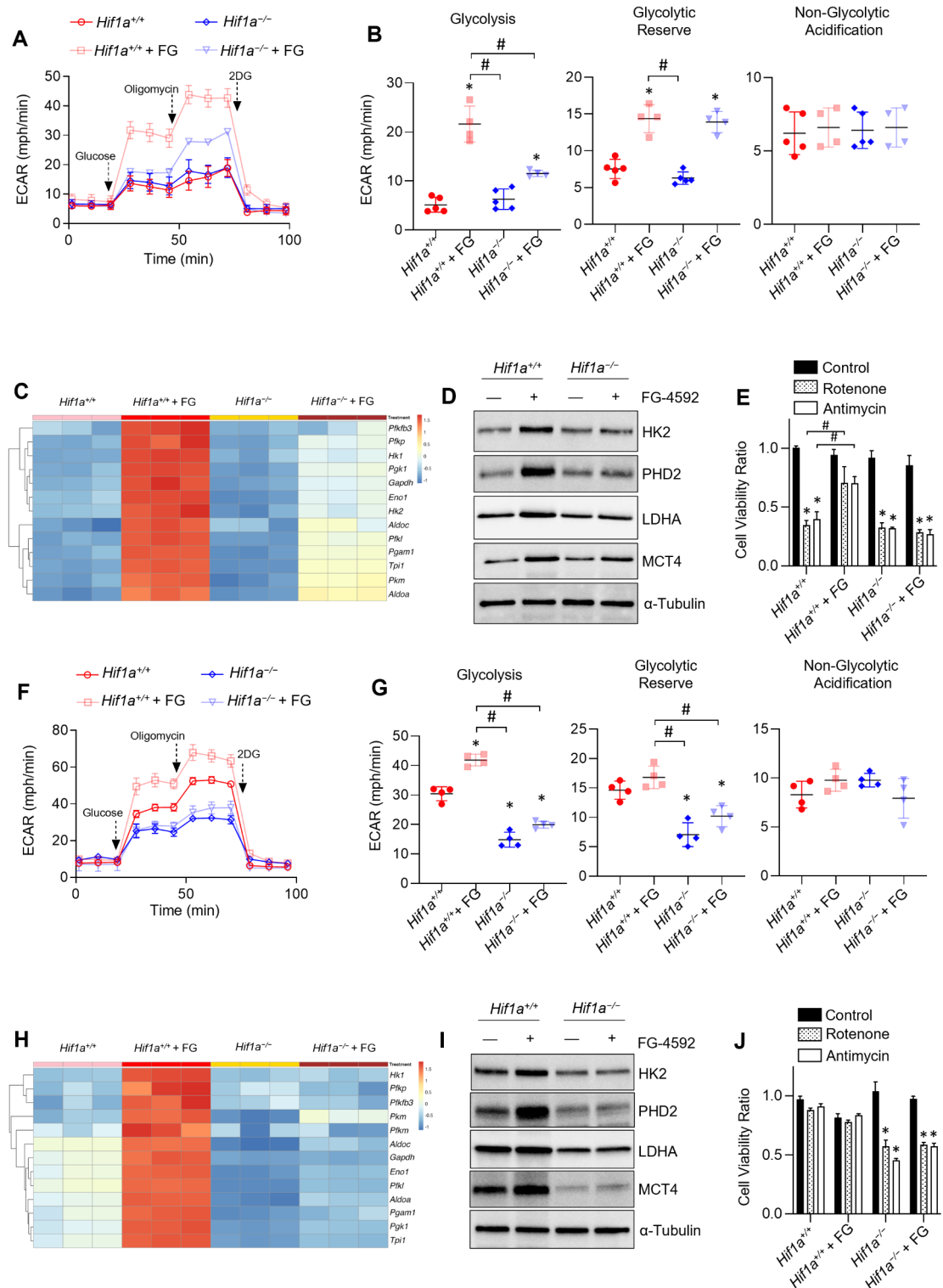


Fig. 1. HIF-1α deletion alters transcriptome both at baseline and following treatment with a HIF-1α stabilizer in BMDMs but only after HIF-1α stabilizer in TR-AMs. TR-AMs (A–C) and BMDMs (D–F) were cultured overnight (16 h) in the presence or absence of FG-4592 (25 μM). (A, D) Western blot analysis of nuclear extracts to verify successful HIF-1α knockout in our transgenic system. (B, E) Clustering of samples based on RNA-seq gene expression profiles using t-SNE projection (C, F) Heatmap analysis of CHEA (ChIP-X Enrichment Analysis) HIF-1α transcription factor targets.



after treatment with FG-4592, $Hif1a^{-/-}$ TR-AMs had significantly lower glycolysis compared to treated TR-AM controls (Fig. 2A, B). Correlating with the low glycolytic rate, both $Hif1a^{+/+}$ and $Hif1a^{-/-}$ TR-AMs had low expression of glycolytic genes and proteins (Fig. 2C, D). Consistent with the role of HIF-1 α in glycolytic gene expression, $Hif1a^{-/-}$ TR-AMs treated with FG-4592 had reduced induction of glycolytic gene and protein expression compared to $Hif1a^{+/+}$ TR-AMs treated with FG-4592 (Fig. 2C, D and Supplementary Fig. 4A). We have previously demonstrated TR-AMs are exquisitely sensitive to inhibition of the ETC and that hypoxic or pharmacological induction of HIF-1 α could rescue TR-AMs treated with mitochondrial ETC inhibitors from cell death¹². In support of these findings, FG-4592 became ineffective in rescuing $Hif1a^{-/-}$ TR-AMs from ETC inhibitor-induced cell death (Fig. 2E).

Our previous work demonstrated that BMDMs have elevated basal levels of HIF-1 α compared with TR-AMs and that hypoxia does not increase the glycolytic rate of these cells. Here, we observed that control BMDMs

◀ **Fig. 2.** HIF-1 α deletion broadly impairs glycolysis in BMDMs but only impairs TR-AM glycolysis following HIF-1 α stabilizer treatment. TR-AMs (A–E) and BMDMs (F–J) were cultured overnight (16 h) in the presence or absence of FG-4592 (25 μ M). (A, F) Using Seahorse XF24 analyzer, glycolysis was measured as extracellular acidification rate (ECAR). Macrophages were treated in succession with glucose, oligomycin (ATP synthase inhibitor) and 2-deoxyglucose (2-DG) (inhibitor of hexokinase 2, or glycolysis). (B, G) Scatter plots quantifying glycolytic parameters. Data represent at least 3 independent experiments ($n=4$ wells per group). Significance determined by two-way ANOVA with Bonferroni's post test. All error bars denote mean \pm SD. Significance markings represented in relation to *Hif1a*^{+/+} no treatment group *, $p<0.05$. Significance markings represented in relation to *Hif1a*^{+/+} + FG-4592 #, $p<0.05$. (C, H) Heatmap of glycolytic specific gene expression in macrophages. (D, I) Western blot analysis of macrophage lysates to assess glycolytic protein expression. (E, J) Macrophages were first treated with FG-4592 for 8 h then treated overnight with mitochondrial inhibitors (500nM Antimycin or 500nM Rotenone). Sulforhodamine B assay was performed to measure cytotoxicity. Graphs represent cell viability compared to control, *Hif1a*^{+/+} no treatment group. Data represent at least 3 independent experiments ($n=3$ per group). All groups compared against *Hif1a*^{+/+} no treatment group with significance determined by two-way ANOVA with Bonferroni's post test. All error bars denote mean \pm SD. *, $p<0.05$ signifies reduced cell viability compared to *Hif1a*^{+/+} no treatment group; #, $p<0.05$ signifies enhanced viability compared to *Hif1a*^{+/+} Rotenone and Antimycin treated groups.

treated with FG-4592 presented with higher ECAR compared to untreated controls (Fig. 2F). However, this increase in BMDMs was more modest (~30%) compared to the 4-fold increase in ECAR following FG-4592 in TR-AMs (Fig. 2A). Glycolytic gene and protein expression (Fig. 2H, I and Supplementary Fig. 4B) were also higher in control BMDMs treated with FG-4592. Glycolytic rates were significantly lower in *Hif1a*^{-/-} BMDMs, and no observable alterations in the ECAR response were seen with FG-4592 treatment. Glycolytic gene and protein expression were also lower in *Hif1a*^{-/-} BMDMs compared to controls and was unaffected by FG-4592 treatment (Fig. 2H, I and Supplementary Fig. 4B). BMDMs are resistant to ETC inhibition-induced death at baseline but they became sensitized after the loss of HIF-1 α (Fig. 2J). These data demonstrate that deletion of HIF-1 α results in impaired glycolysis in both TR-AMs and BMDMs. Consistent with our previous findings that TR-AMs contain very little expression of HIF-1 α protein at baseline, we found that loss of HIF-1 α does not affect glycolysis in TR-AMs at baseline and affects glycolysis only after treatment with FG-4592. BMDMs, which have high basal levels of HIF-1 α exhibited reduction in glycolysis following the loss of *Hif1a* both at baseline and after FG-4592 suggesting that HIF-1 α regulates metabolic function in BMDMs both in normoxia as well as during prolyl hydroxylase inhibition.

HIF-1 α deletion boosts mitochondrial function in BMDMs but has limited impact on TR-AM mitochondrial function

The effects of HIF-1 α deletion on glycolytic function and inflammation have been well-described in BMDMs, but little is known about how HIF-1 α deletion impacts mitochondrial function in macrophages¹⁵. To determine how HIF-1 α regulates mitochondrial function, we performed a mitochondrial stress test and found that *Hif1a*^{-/-} TR-AMs exhibited basal oxygen consumption rates (OCRs) comparable to untreated controls (Fig. 3A, B). FG-4592 treated control *Hif1a*^{+/+} TR-AMs exhibited reduced basal OCR, suggesting a shift toward glycolytic ATP production, but they were still able to reach maximal oxygen consumption under FCCP stimulation. This glycolytic shift was confirmed by the reciprocal change in ECAR measurement where control *Hif1a*^{+/+} TR-AMs treated with FG-4592 no longer exhibited reduction in ECAR following rotenone and antimycin A injection whereas *Hif1a*^{-/-} TR-AMs treated with FG-4592 showed a reduction in ECAR (Supplementary Fig. S5). Carbonic acid derived from mitochondrial CO₂ can be measured as the ECAR during mitochondrial stress test²⁰. The reduction in *Hif1a*^{-/-} TR-AMs ECAR after administration of rotenone and antimycin A support the notion that the ECAR is mitochondria-derived carbonic acid, while a lack of ECAR responsiveness in control *Hif1a*^{+/+} TR-AMs signifies glycolytically produced acid. Interestingly, while *Hif1a*^{-/-} TR-AMs have higher maximal respiration/spare capacity compared to controls, changes in maximal oxygen consumption appear to have little functional consequence under normal, non-stressed conditions.

Unlike TR-AMs, control BMDMs treated with FG-4592 showed diminished OCR across all parameters compared to untreated controls. HIF-1 α deletion in BMDMs led to significantly higher basal respiration and ATP production compared to controls and the effect of FG-4592 on OCR was greatly diminished (Fig. 3C, D). In agreement with the OCR data, GC-MS analysis showed that key TCA cycle metabolites were significantly elevated in *Hif1a*^{-/-} BMDMs, and that the levels of these metabolites were less responsive to FG-4592 treatment compared to controls (Fig. 3E).

To bolster our mitochondrial stress test and GC-MS data, we performed western blot analysis using an antibody cocktail that recognizes components of each of the respiratory complexes. *Hif1a*^{-/-} TR-AMs did not exhibit any significant alterations in ETC complex protein expression compared to controls, and FG-4592 had no effect on ETC protein expression across all groups (Fig. 4A). Heatmap analysis of respiratory subunit gene expression revealed that FG-4592 reduced the expression of ETC genes in control *Hif1a*^{+/+} TR-AMs, and that this response was not observed in *Hif1a*^{-/-} TR-AMs treated with FG-4592 (Fig. 4B). Unlike TR-AMs, HIF-1 α deletion in BMDMs led to significant increases in protein expression for ETC complexes I–IV (Fig. 4C and Supplementary Fig. 6). FG-4592 did not alter ETC protein expression in control or *Hif1a*^{-/-} BMDMs. Like control TR-AMs, FG-4592 reduced ETC gene expression in control BMDMs, but did not affect ETC gene expression in *Hif1a*^{-/-} BMDMs (Fig. 4D). *Hif1a*^{-/-} BMDMs also had higher basal ETC gene expression than controls correlating with their protein expression data.

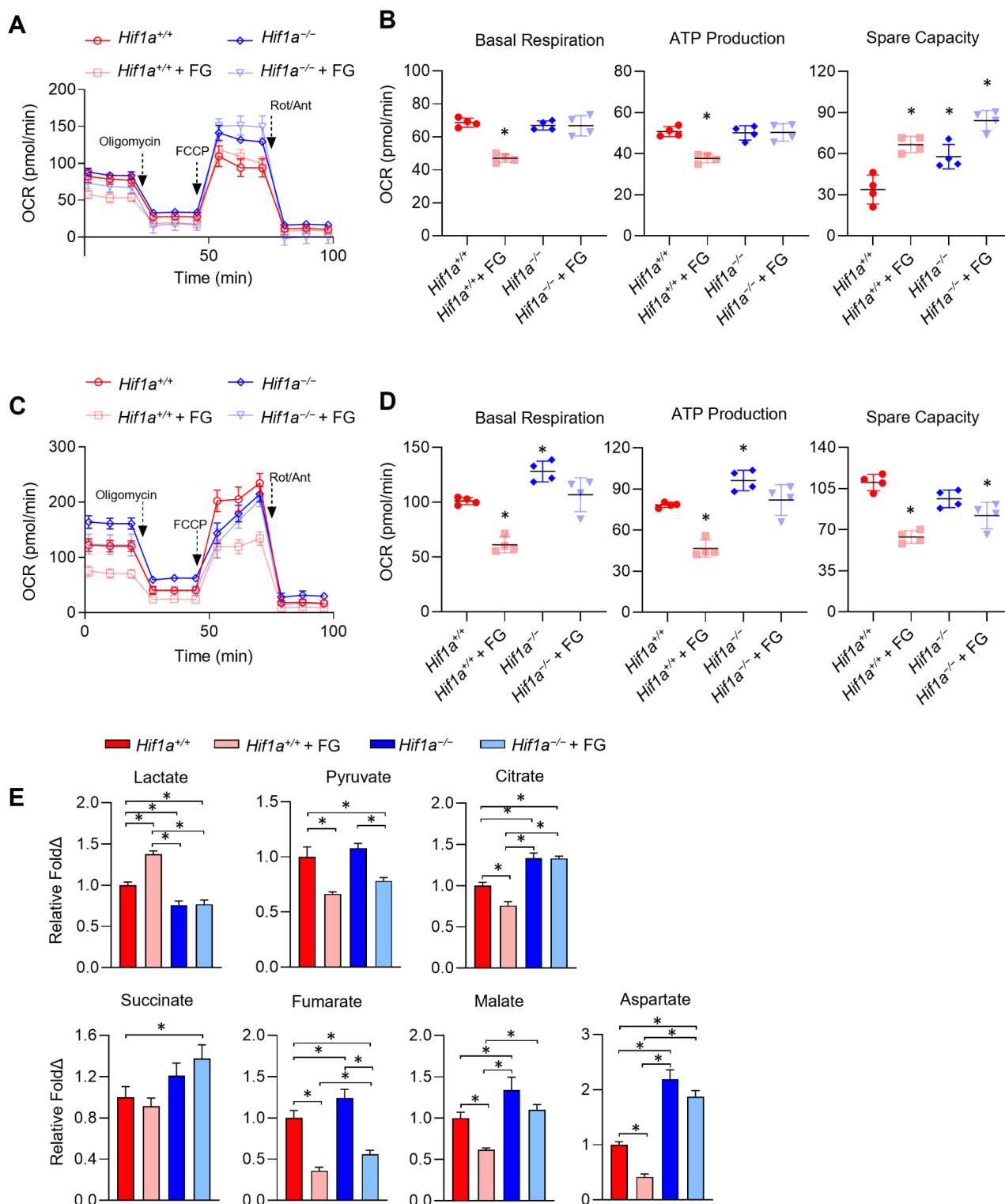


Fig. 3. HIF-1 α deletion boosts mitochondrial function in BMDMs but has limited impact on TR-AM mitochondrial function. TR-AMs (A, B) and BMDMs (C–E) were cultured overnight (16 h) in the presence or absence of FG-4592 (25 μ M). (A, C) Mitochondrial stress test to measure oxygen consumption rate (OCR) using Seahorse XF24 in TR-AMs and BMDMs. Macrophages were treated sequentially with oligomycin (ATP synthase inhibitor), FCCP (uncoupler) and Rotenone/Antimycin A (complex I and III inhibitor, respectively). (B, D) Interleaved scatter plots quantifying mitochondrial respiration parameters. Data represents at least 3 experiments ($n=4$ separate wells per group). Mitochondrial parameters were compared against *Hif1a*^{+/+} no treatment group. Significance was determined by two-way ANOVA with Bonferroni's post test. (E) GC-MS metabolite analysis of BMDMs. Data represent at least 3 independent experiments ($n=3$ replicates per experimental condition). All groups compared against *Hif1a*^{+/+} no treatment group with significance determined by two-way ANOVA with Bonferroni's post test. All error bars denote mean \pm SD. *, $p < 0.05$.

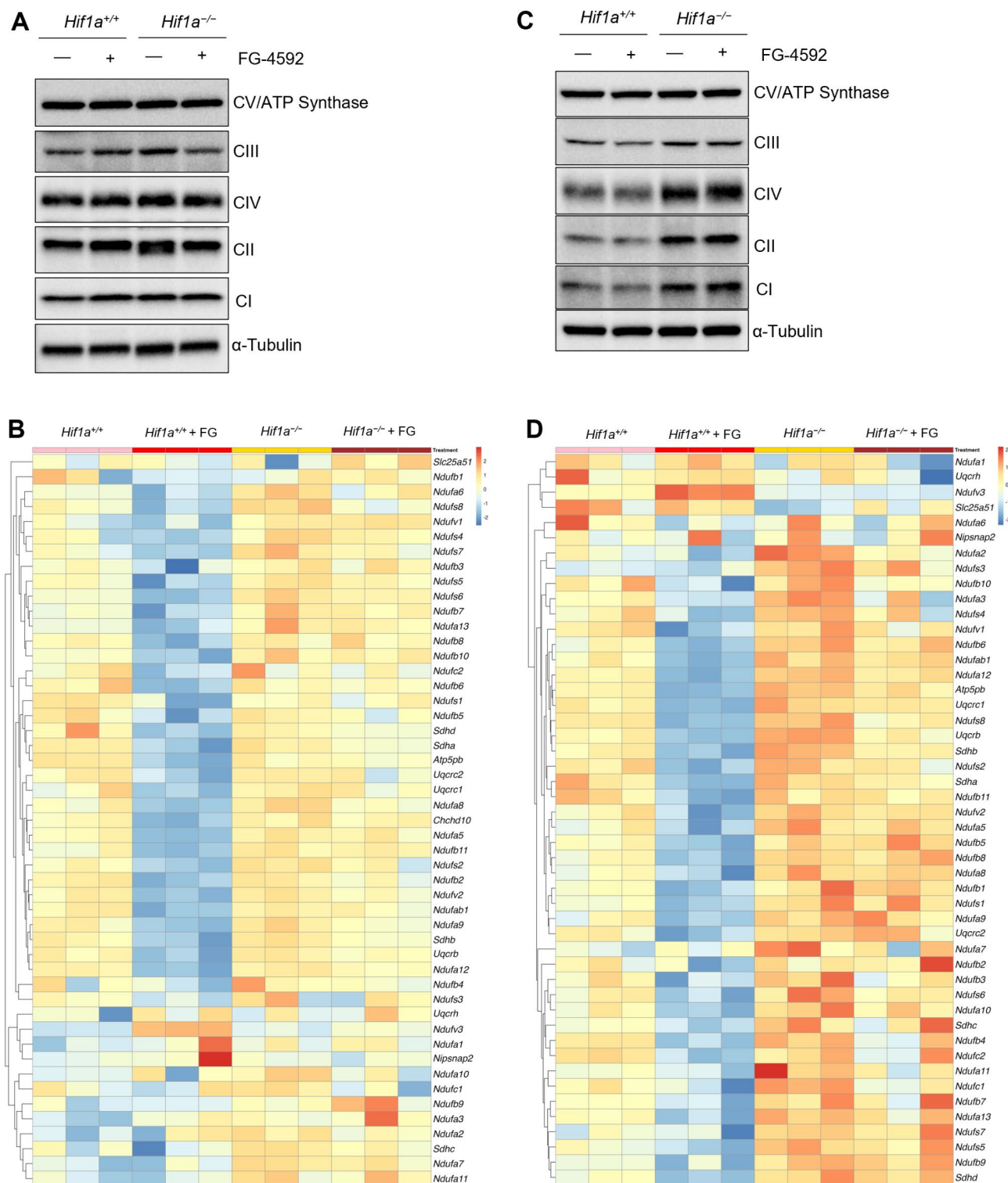
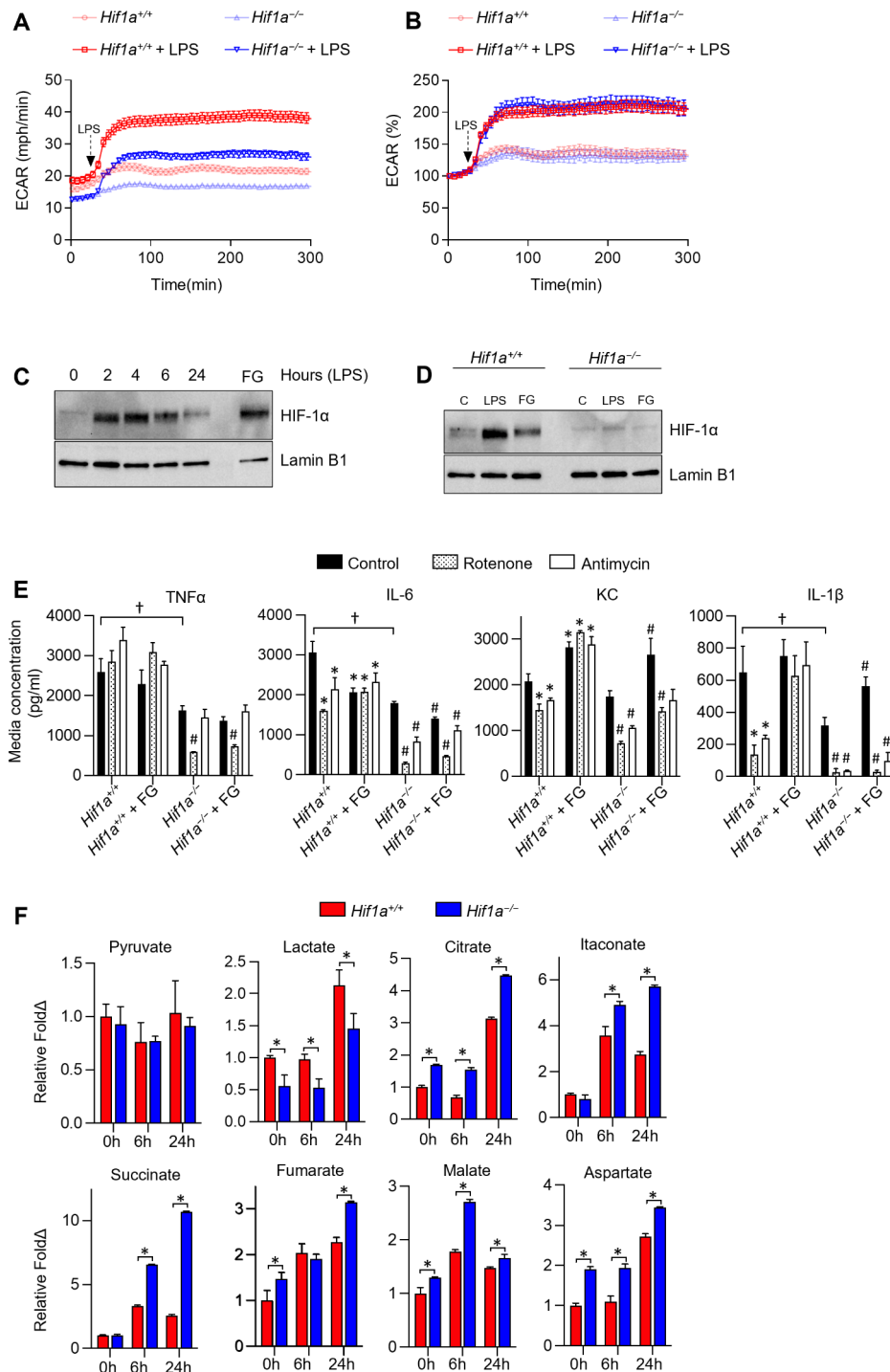


Fig. 4. HIF-1 α deletion results in increased mitochondrial gene and protein expression in BMDMs, but not TR-AMs. TR-AMs (A-B) and BMDMs (C-D) were cultured overnight (16 h) in the presence or absence of FG-4592 (25 μ M). (A, C) Western blot analysis of macrophage lysates to assess electron transport chain protein expression. (B, D) Heatmap of gene expression related to oxidative phosphorylation.

Taken together, these data suggest that HIF-1 α serves as a negative regulator of mitochondrial function in BMDMs under steady-state conditions. Moreover, HIF-1 α stabilization reduces ETC-related gene expression in both TR-AMs and BMDMs, but this does not correlate with the reduction in ETC protein expression, which remains unchanged in the presence of FG-4592.



HIF-1α deletion impairs inflammatory capacity in BMDMs, but not in TR-AMs

The central role of HIF-1α in macrophage inflammation has been well-documented²¹. Here, we wanted to determine more thoroughly the metabolic and inflammatory alterations that occur in the absence of HIF-1α. We and others have shown the immediate upregulation of glycolysis upon LPS exposure in BMDMs^{9,22,23}. To determine if the increase in glycolytic output was mediated by HIF-1α, we treated *Hif1a*^{-/-} BMDMs and controls with LPS to observe changes in ECAR over a five-hour period. Figure 5A shows that *Hif1a*^{-/-} BMDMs still respond to LPS by immediately upregulating glycolysis. This response is attenuated compared to controls, which is likely a result of *Hif1a*^{-/-} BMDMs having lower glycolytic gene and protein expression (Fig. 2H, I). While basal ECAR was lower in *Hif1a*^{-/-} BMDMs compared to controls, there was no change in the magnitude of glycolytic induction when the ECAR was normalized to percent change (ECAR %) from baseline (Fig. 5B). This would suggest that HIF-1α is not required for the enhanced glycolysis observed under LPS stimulation. In

◀ **Fig. 5.** HIF-1 α deletion impairs inflammatory capacity in BMDMs. (A, B) ECAR was measured following acute LPS injection (final concentration: 20 ng/ml) in BMDMs. ECAR data represented both as (A) raw values and (B) % change from baseline. Data represent at least 3 independent experiments ($n = 4$ separate wells per group). Error bars denote mean \pm SEM to allow for easier visualization of line graphs. (C) Western blot analysis assessing nuclear localization of HIF-1 α over 24 h LPS (20ng/ml) time course. FG-4592 (FG) was used as a positive control for HIF-1 α protein expression. (D) Western blot analysis assessing nuclear localization of HIF-1 α in *Hif1a*^{+/+} and *Hif1a*^{-/-} BMDMs at 4 h after LPS or FG verifying the loss of expression of HIF-1 α in *Hif1a*^{-/-} BMDMs at baseline and loss of induction of HIF-1 α following LPS and FG. (E) BMDMs were treated overnight with FG-4592 (25 μ M) and then challenged with LPS (20ng/ml) in the presence or absence of Antimycin A (20nM) or Rotenone (20nM) for 6 h and secreted cytokines were measured via ELISA. Significance determined by two-way ANOVA with Bonferroni's post test. All error bars denote mean \pm SD. Significance markings represented in relation to *Hif1a*^{+/+} LPS only group with †, $p < 0.05$. *, $p < 0.05$ denotes significance in relation to *Hif1a*^{+/+} LPS only group within respective genotype. #, $p < 0.05$ denotes significance in relation to *Hif1a*^{-/-} LPS only group within respective genotype. (F) GC-MS metabolite analysis of BMDM LPS (20ng/ml) time course. Data represent at least 3 independent experiments ($n = 3$ replicates per experimental condition). Significance determined by two-way ANOVA with Bonferroni's post test. All error bars denote mean \pm SD. Significance markings represented in relation to *Hif1a*^{+/+} vs. *Hif1a*^{-/-} at a given timepoint with *, $p < 0.05$.

agreement with these data, the small interfering RNA (siRNA) knockdown of *Hif1a* in BMDMs did not alter glycolytic responsiveness to LPS (Supplementary Fig. 7A–C). The glycolytic rates of *Hif1a*^{-/-} and control TR-AMs remained unresponsive to LPS injection, which is consistent with our previous findings (Supplementary Fig. S7D)⁹.

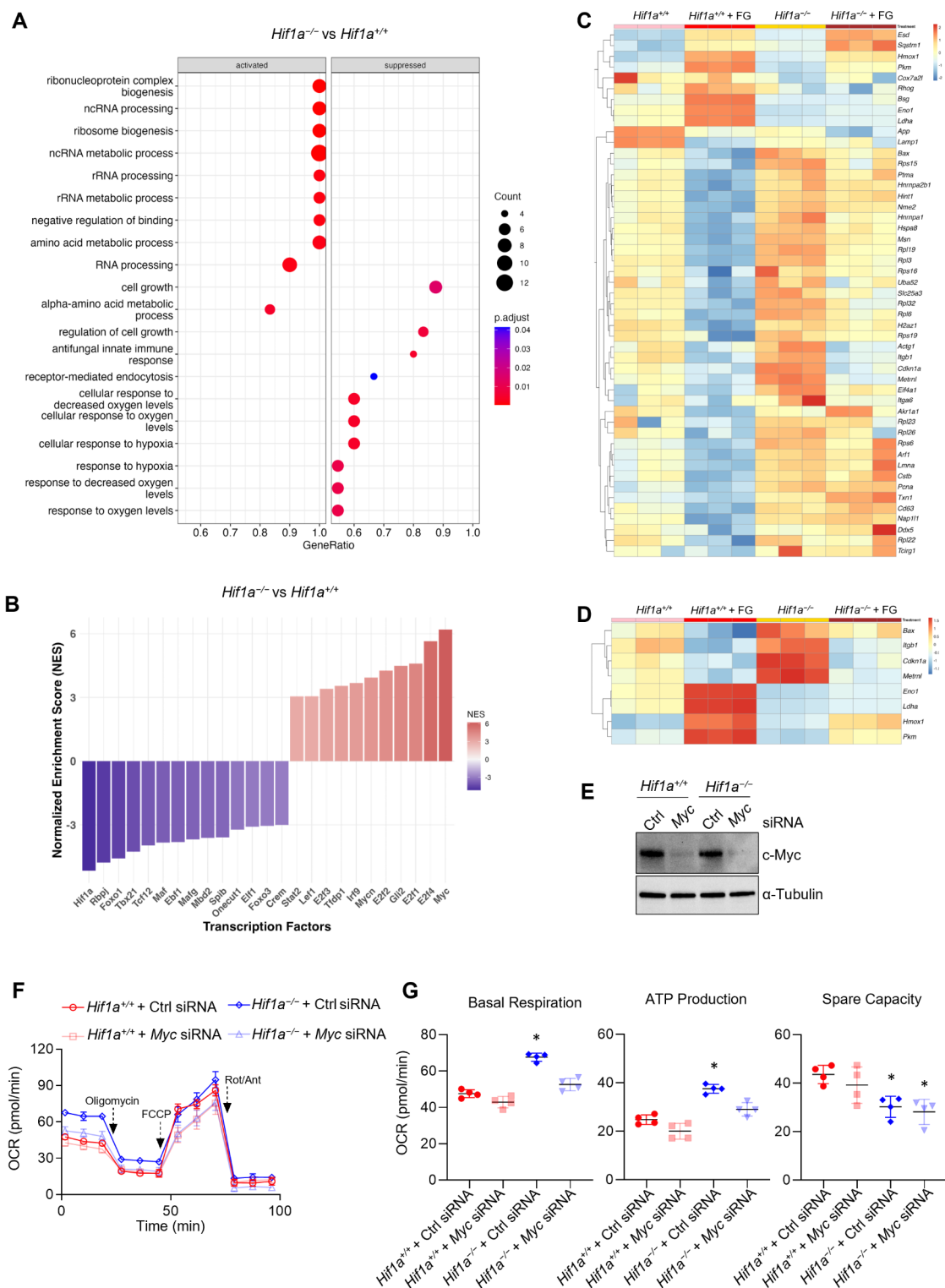
We next examined the nuclear localization of HIF-1 α in macrophages following LPS treatment. Several reports have shown HIF-1 α protein stabilization in the presence of LPS, but the exact time-course of stabilization remains unclear. We found that nuclear stabilization of HIF-1 α in BMDMs occurs early in exposure, peaks around 4 h, and returns to near baseline levels by 24 h (Fig. 5C). We confirmed the loss of HIF-1 α protein in our *Hif1a*^{-/-} BMDMs under LPS stimulation by verifying the lack of nuclear expression using western blot (Fig. 5D) and immunofluorescence (Supplementary Fig. S8). Moreover, we have observed HIF-1 α induction in TR-AMs under hypoxia or pseudohypoxia (prolyl hydroxylase inhibition with FG-4592), but we have not seen HIF-1 α induction/stabilization in TR-AMs under inflammatory stimuli. Immunofluorescence and western blot confirmed these observations where HIF-1 α was only observed in the presence of FG-4592 in TR-AMs, but not in the presence of LPS (Supplementary Fig. S9, S10). Poly (I:C), a potent TLR3 antagonist, also failed to induce HIF-1 α in TR-AMs.

We next sought to determine the effect of HIF-1 α deletion on macrophage cytokine production. To do so, macrophages were preconditioned overnight with FG-4592 and then subsequently treated with LPS for 6 h in the presence or absence of ETC inhibitors (rotenone or antimycin A). This allowed us to assess both the general role of HIF-1 α in inflammation and the reliance of cells on glycolysis for inflammation under ETC inhibition. Compared to control BMDMs, *Hif1a*^{-/-} BMDMs secreted less TNF α , IL-6, and IL-1 β in response to LPS and exhibited reduced cytokine secretion in the presence of an ETC inhibitor (Fig. 5E). FG-4592 appeared to increase KC and IL-1 β secretion and decrease IL-6 secretion independently of HIF-1 α deletion in BMDMs. Moreover, FG-4592 failed to rescue rotenone-induced reduction in all measured cytokines and failed to reverse the antimycin A-induced reduction in IL-1 β and KC secretion in *Hif1a*^{-/-} BMDMs. By contrast, TR-AM cytokine secretion was unperturbed by HIF-1 α deletion, and both *Hif1a*^{-/-} and control TR-AMs were equally susceptible to ETC inhibitor-induced cytokine impairments. (Supplementary Fig. S11A). HIF-1 α deletion only became a factor in cytokine secretion when TR-AMs were preconditioned with FG-4592 to induce glycolysis. In this case, the cytokine impairment from ETC inhibition was dramatically reversed in control TR-AMs, but not in *Hif1a*^{-/-} TR-AMs.

Next, BMDMs and TR-AMs were treated with LPS for 6 and 24 h and the cellular extracts were analyzed via GC-MS. As expected, *Hif1a*^{-/-} BMDMs had reduced lactate production in response to LPS (Fig. 5F). While pyruvate levels remained unchanged, all other TCA cycle metabolites were significantly elevated in *Hif1a*^{-/-} BMDMs treated with LPS compared to controls. Most notably, succinate, citrate, and itaconate, which are known regulators of macrophage inflammation, were robustly elevated in *Hif1a*^{-/-} BMDMs. HIF1 α deletion in TR-AMs had negligible effects on LPS-induced metabolite levels (Supplementary Fig. S11B). Malate was the only TCA cycle metabolite that was elevated in *Hif1a*^{-/-} TR-AMs compared to controls. These data indicate that HIF-1 α deletion in BMDMs leads to reduced cytokine production and elevated TCA cycle metabolite levels in response to LPS.

HIF-1 α deletion in BMDMs alters c-Myc transcriptional activity

Thus far, we have demonstrated that HIF-1 α is required for TR-AM glycolytic adaptation under prolyl hydroxylase inhibition, but otherwise HIF-1 α is dispensable for TR-AM inflammatory processes under steady-state conditions. This is not the case in BMDMs where HIF-1 α deletion broadly impacts metabolism and effector function. More specifically, *Hif1a*^{-/-} BMDMs have reduced glycolytic and inflammatory capabilities but have enhanced mitochondrial function. By performing Gene Ontology-Biological Processes (GO-BP) enrichment analysis, we sought to identify regulatory pathways within our RNA-seq dataset that could explain the altered phenotype in *Hif1a*^{-/-} BMDMs. Predictably, GO-BP analysis revealed suppression of biological processes related to hypoxia and oxygen responsiveness in *Hif1a*^{-/-} BMDMs (Fig. 6A). HIF-1 α deletion led to the activation of biological processes related to ribosome biogenesis, ribosomal RNA processing, and cell growth²⁴. To determine



what controls the transcriptional responses in the absence of HIF-1 α , we used an unbiased approach using the DoRothEA mouse regulon transcription factor (TF) enrichment computation to estimate the activity of TFs in gene expression data, to understand how TFs drive gene expression changes in a given biological context²⁵. Not surprisingly, the HIF-1 α regulon genes had the most negative enrichment score in our *Hif1a*^{-/-} BMDMs (Fig. 6B). In contrast, Myc was the most positively enriched regulatory interaction with its targets in *Hif1a*^{-/-} BMDMs (Fig. 6B).

It is well-known that c-Myc often works diametrically opposed to HIF-1 α and promotes cell proliferation and growth, which were the biological processes that were activated following HIF-1 α deletion²⁶. Thus, we queried c-Myc target genes to assess c-Myc transcriptional activity and found that *Hif1a*^{-/-} BMDMs had higher gene expression for the majority of c-Myc targets (Fig. 6C), with several of the genes being related to enhanced translational activity and cell proliferation (*Cdkn1a* and *Pcna*). Moreover, the only c-Myc targets that were

◀ **Fig. 6.** HIF-1 α deletion in BMDMs alters c-Myc transcriptional activity. **(A)** GO-BP enrichment analysis of gene sets comparing *Hif1a*^{-/-} vs. *Hif1a*^{+/+} BMDMs at baseline. **(B)** Transcription factor enrichment was computed using the DoRothEA R tool with significant differentially expressed genes ($\log_{2}FC \leq 1$, $p \leq 0.05$) for *Hif1a*^{-/-} vs. *Hif1a*^{+/+} BMDMs comparisons at baseline. The color legend indicates TF activity. **(C)** Heatmap of significantly expressed c-Myc target genes and **(D)** Heatmap of shared target genes of c-Myc and HIF-1 α comparing *Hif1a*^{+/+} and *Hif1a*^{-/-} BMDMs \pm FG-4592 (25 μ M) for 16 h. All represented DEGs had gene expression abundances exceeding 200 counts. **(E–G)** BMDMs were electroporated with non-targeting (Ctrl) or *Myc* siRNA. Cells were allowed to rest for 48 h then subjected to western blot or seahorse analysis. **(E)** Western blot confirming successful knock down of *Myc*. **(F)** Mitochondrial stress test to measure oxygen consumption rate (OCR) in BMDMs. Macrophages were treated sequentially with oligomycin (ATP synthase inhibitor), FCCP (uncoupler) and Rotenone/Antimycin A (complex I and III inhibitor, respectively). **(G)** Interleaved scatter plots quantifying mitochondrial respiration parameters. Data represents at least 3 experiments ($n = 4$ separate wells per group). Mitochondrial parameters were compared against *Hif1a*^{+/+} Ctrl siRNA group and significance was determined by two-way ANOVA with Bonferroni's post test.

downregulated in *Hif1a*^{-/-} compared to controls were genes related to glycolysis, and these genes have been identified as shared c-Myc and HIF-1 α targets (Fig. 6D). This observation supports our data that HIF-1 α , and not c-Myc, is the primary regulator of glycolysis in BMDMs. Thus, with the deletion of HIF-1 α in BMDMs, it is possible that c-Myc shifts BMDMs toward a mitochondrial dominated metabolism. To assess these observations, we performed siRNA knockdown of *Myc* and found that *Myc* knockdown in *Hif1a*^{-/-} BMDMs reduced basal respiration and ATP production to levels comparable to control BMDMs (Fig. 6E–G). This suggests that *Myc* is responsible for increased mitochondrial activity in the absence of HIF-1 α .

Discussion

Macrophages are highly plastic in their responses to immune stimuli. Their proinflammatory processes are necessary for pathogen clearance, while their pro-resolving properties are required in tissue repair and disease resolution. We now know that tissue-specificity is a key determinant for macrophage function. The respiratory tract is the primary portal for pathogen entry into the human body, and acute respiratory distress syndrome (ARDS) caused by influenza virus and SARS-CoV-2 causes significant mortality annually. TR-AMs play a critical role in mediating the response to these viruses as loss of TR-AMs during ARDS is associated with more severe disease and higher morbidity and mortality^{27–29}. Moreover, recruitment of non-resident macrophages to the lung during ARDS is thought to worsen outcomes^{30,31}. Thus, understanding fundamental macrophage processes, such as metabolic adaptation to immune stimuli and local tissue conditions could ultimately lead to new therapeutic strategies to attenuate disease.

We have previously shown that TR-AMs have very low glycolytic activity under steady-state conditions and that glycolysis is dispensable for LPS-induced inflammation in these cells⁹. We then went on to show that TR-AMs could undergo glycolytic reprogramming at low oxygen concentrations, and that HIF-1 α was likely driving this metabolic switch. Treating influenza-infected mice with prolyl hydroxylase inhibitor, FG-4592, promoted TR-AM survival and reduced lung injury¹². Together, these previous findings demonstrate that HIF-1 α induction in TR-AMs provides a mechanism for cell survival in an injured, hypoxic lung. In this study, we wanted to definitively identify HIF-1 α as the driver of glycolytic adaptation in TR-AMs and to rule out HIF-1 α as a mediator of TR-AM inflammation. Moreover, we wanted to provide new insight into the central role of HIF-1 α in BMDM effector function. To do so, we generated HIF-1 α knockout macrophages and found that HIF-1 α is not required for steady-state TR-AM function, but it is only required for glycolytic adaptation under prolyl hydroxylase inhibition. RNA-seq analysis revealed *Hif1a*^{-/-} TR-AMs had only 10 DEGs compared to controls at steady-state, but 610 DEGs were observed between control and *Hif1a*^{-/-} TR-AMs treated with FG-4592. These data were in line with glycolysis stress test and glycolytic protein expression data, and ETC inhibitor-induced cytotoxicity experiments in which *Hif1a*^{-/-} TR-AMs failed to undergo glycolytic adaptation in the presence of FG-4592, and thus remained highly susceptible to ETC inhibitor-induced cell death. These data suggest that HIF-1 α plays only a minor role in steady-state, terminally differentiated TR-AMs, which is in agreement with the findings that HIF-1 α target genes are significantly downregulated in TR-AMs during postnatal maturation¹⁹.

In contrast, *Hif1a*^{-/-} BMDMs exhibited significant alterations at steady-state, presenting with 305 DEGs compared to controls, and the differences increased to 1022 DEGs when treated with FG-4592 (*Hif1a*^{+/+} + FG-4592 vs. *Hif1a*^{-/-} + FG-4592). These data are in line with previous work describing HIF-1 α regulation of basal glycolytic metabolism in mouse peritoneal macrophages¹⁵. *Hif1a*^{-/-} BMDMs also exhibited decreased glycolytic output and protein expression and became susceptible to ETC inhibition-induced cell death. FG-4592 treatment had no functional effect on glycolytic parameters in *Hif1a*^{-/-} BMDMs. In control BMDMs, prolyl hydroxylase domain protein 2 (PHD2) and monocarboxylate transporter 4 (MCT4) protein expression increased with FG-4592 treatment, while lactate dehydrogenase A (LDHA) and hexokinase 2 (HK2) remained unchanged. As we have previously shown, control BMDMs are inherently glycolytic so upregulation of HK2 and LDHA with FG-4592 provides little metabolic advantage^{9,12}. Increased PHD2 upregulation in BMDMs is likely a response to increased HIF-1 α stabilization given that PHD2 is a key enzyme in marking HIF-1 α for proteasomal degradation. Increased MCT4 may be necessary to export the increased lactate/acid produced by BMDMs treated with FG-4592. Overall, our findings demonstrate that *Hif1a*^{-/-} BMDMs more closely resemble control TR-AMs with regards to glycolytic phenotype, and that HIF-1 α is required for normal BMDM metabolic function.

When assessing mitochondrial function in our *Hif1a*^{-/-} macrophages, we found that TR-AMs had minimal alterations compared to controls. *Hif1a*^{-/-} TR-AMs only showed a slight elevation in spare mitochondrial

capacity, but no change in basal respiration or ATP production. In contrast, *Hif1a*^{-/-} BMDMs maintained higher basal oxygen consumption rates and ATP production, and OCR was less affected by FG-4592 treatment under mitochondrial stress test assessment. Interestingly, reciprocal ECAR measurements, while generally lower in *Hif1a*^{-/-} BMDMs, remained mostly unresponsive to mitochondrial inhibitors (rotenone and antimycin A). This suggests that *Hif1a*^{-/-} BMDMs still maintain the ability to produce significant amounts of glycolysis-derived lactate under ETC inhibition, but this does not appear to be sufficient to overcome ETC inhibitor-induced cellular cytotoxicity. It may be that in the absence of HIF-1 α other transcription factors aid in the basal maintenance of BMDM glycolysis, but that HIF-1 α is required for a fully functional glycolytic phenotype^{32–35}. This is not the case in untreated TR-AMs where their reciprocal ECAR measurements return to basal levels regardless of HIF-1 α deletion suggesting that acidification measurements represent mitochondrial-derived CO₂²⁰. Only when control *Hif1a*^{+/+} TR-AMs are treated with FG-4592 does their reciprocal ECAR measurements become unresponsive to rotenone and antimycin A suggesting a dominant glycolytic phenotype.

HIF-1 α deletion in BMDMs resulted in higher TCA cycle metabolite levels, which correlated with increased gene and protein expression of ETC. In contrast, HIF-1 α deletion had no impact on ETC protein or gene expression in TR-AMs. FG-4592 treatment led to downregulation of ETC genes in control TR-AMs and BMDMs, but this effect was lost when HIF-1 α was deleted. This suggests that HIF-1 α is responsible for the transcriptional downregulation of ETC genes under prolyl hydroxylase inhibition regardless of macrophage origin. Despite its effect on ETC gene expression, FG-4592 did not significantly affect ETC protein expression. The lack of a significant change in ETC protein expression despite a substantial reduction in gene expression after FG-4592 is likely due to insufficient mitochondria turnover during the course of our experiment for loss of protein expression to manifest. ETC protein expression may be more stable and therefore remain unperturbed by FG-4592 treatment in either cell type in the short-term. Based on these data, it is possible that loss of HIF-1 α in BMDMs enhances mitochondrial capabilities as compensatory mechanism for deficiencies in glycolysis or that the presence of HIF-1 α serves as negative regulator of mitochondrial function. As a result, *Hif1a*^{-/-} BMDM metabolism resembles that of control TR-AMs in their glycolytic deficiency and enhanced mitochondrial metabolism.

It is well-documented that HIF-1 α is a key mediator of inflammation in macrophages of monocytic origin and that glycolytic flux increases immediately following exposure to proinflammatory immune stimulus^{9,15,22,23}. Here, we show that HIF-1 α is not responsible for the increased glycolytic flux under LPS stimulation in BMDMs. *Hif1a*^{-/-} BMDMs had lower basal ECAR rates under LPS stimulus, but the magnitude of the response in ECAR after LPS was comparable to control BMDMs. Similarly, siRNA knockdown of *Hif1a* in BMDMs had no impact on the glycolytic ECAR flux in response to LPS. The siRNA knockdown of *Hif1a* also did not affect basal ECAR. This indicates that the glycolytic phenotypes of *Hif1a*^{-/-} BMDMs and HIF-1 α siRNA knockdown BMDMs are different. *Hif1a*^{-/-} results in lower glycolytic capacity and protein expression. siRNA knockdown greatly reduces HIF-1 α expression but does not alter glycolytic phenotype¹². The short-time course of a knockdown experiment was likely insufficient to allow the cells reprogram towards a more mitochondrial phenotype that is less dependent on glycolysis. Our data suggest that the increase of glycolytic flux in response to LPS is independent of HIF-1 α . Although LPS induces glycolytic gene expression hours after treatment, it is likely that these alterations have little impact on the immediate alterations in glycolytic flux. It is thus more likely that LPS increases the activity of rate-limiting enzymes in the glycolytic pathway, such as 6-Phosphofructo-2-Kinase/Fructose-2,6-Biphosphatase 3 (PFKFB3) or pyruvate kinase M2 (PKM2), to enhance glycolytic flux^{16,36,37}. We also observed broad decreases in cytokine production in *Hif1a*^{-/-} BMDMs in response to LPS. Others have shown that HIF-1 α deletion results in deficiencies related to IL-1 β production, and that HIF-1 α activates NF- κ B^{16,18,38,39}. Our findings indicate that broad reductions in cytokine production are likely a result of glycolytic deficiency in *Hif1a*^{-/-} BMDMs. Alternatively, in the absence of HIF-1 α , BMDMs have elevated TCA cycle metabolite production in response to LPS, including the immunoregulatory metabolite itaconate, which may dampen the immune response^{40–43}. Similarly, our data indicate that *Hif1a*^{-/-} BMDMs have elevated citrate levels both at steady-state and following LPS treatment. Aside from its traditional role in the TCA cycle, citrate can be exported from the mitochondria to generate acetyl-CoA, which can be used for *de novo* fatty acid synthesis or epigenetic modifications^{44–46}. Others have reported that anti-inflammatory macrophage function relies predominantly on mitochondrial metabolic pathways, which would be in agreement with the enhanced mitochondrial function and reduced proinflammatory cytokine production observed in our *Hif1a*^{-/-} BMDMs.⁴⁷

We observed no changes in TR-AM inflammatory capabilities upon HIF-1 α deletion. ETC inhibition greatly reduces cytokine production in TR-AMs, but these reductions can be overcome through pretreatment with hypoxia¹². These findings are aligned with our data showing that unlike BMDMs, LPS treatment does not result in HIF-1 α translocation to the nucleus in TR-AMs. Zhu and colleagues have shown that Poly (I: C) or influenza infection upregulate HIF-1 α in TR-AMs, but we were not able to replicate these results^{48,49}. We find that only hypoxia or pharmacological inhibition of prolyl hydroxylases induces HIF-1 α in TR-AMs. One explanation for the observed differences is that Zhu and colleagues cultured TR-AMs in the presence of GM-CSF. GM-CSF is important to TR-AM function in vivo, but it induces proliferation of TR-AMs in culture^{50,51}. Within the alveolus, epithelial-derived soluble mediators and direct interactions with epithelial cells function to prevent widespread TR-AM proliferation in the presence of physiological levels of GM-CSF⁵². Thus, it may be that previous observations of HIF-1 α induction in TR-AMs are related to proliferation as opposed to inflammatory effector function.

While HIF-1 α deletion in BMDMs depressed proinflammatory effector function, RNA-seq Gene Ontology analysis showed upregulation in ribosomal biogenesis, rRNA metabolic processes, and noncoding RNA processing gene pathways in *Hif1a*^{-/-} BMDMs. Others have recently observed upregulation of ribosomal biogenesis genes in tumor-associated macrophages, but the mechanism underlying this phenomenon remains unclear⁵³. Increased expression of these gene pathways has been associated with increased proliferation and cell

growth, and c-Myc has been identified as a critical regulator of these processes²⁴. c-Myc and HIF-1 α can work in concert or opposition to augment cellular metabolism, protein synthesis, cell growth, and proliferation²⁶. While it may seem paradoxical, *Hif1a*^{-/-} tumors grow faster and become more invasive in the presence of adequate oxygen, but under hypoxia, HIF-1 α can displace c-Myc from DNA to induce cell cycle arrest^{54,55}. In a similar vein, BMDMs restimulated with MCSF following a period of starvation upregulate c-Myc and shift toward a proliferative phenotype reliant on both glycolysis and mitochondrial metabolism. LPS treatment downregulates c-Myc, upregulates HIF-1 α , and supports a glycolysis dominant metabolism in BMDMs⁵⁶. This suggests that BMDMs proinflammatory effector function suppresses proliferation and shifts the cell from Myc-dependent to HIF-1 α -dependent metabolism. We find the Myc regulon to be the most upregulated transcriptional network in *Hif1a*^{-/-} BMDMs compared to controls. This suggests that c-Myc serves a more dominant role in the absence of HIF-1 α . This likely explains the upregulation of ETC protein expression and pathways involved in ribosomal biogenesis in our *Hif1a*^{-/-} BMDMs. Without HIF-1 α , c-Myc can serve a larger role in shaping BMDM metabolism, which fundamentally changes how BMDMs respond to immune stimulus. Like Myc, the upregulation of other regulons, including *E2f1-4*, *Lef1*, *Gil2*, and *Tfdp1*, point towards a pro-growth phenotype in *Hif1a*^{-/-} BMDMs.^{57–59} DoRothEA analysis revealed the downregulation of *Foxo*, *Tcf12*, *Maf*, and *Onecut* in *Hif1a*^{-/-} BMDMs. These regulons are associated with glucose homeostasis and cell cycle arrest^{60–62}. Other downregulated regulons included *Rbpj*, *Tbx21*, *Mbd2*, *Spib* and *Crem*, which have been identified as regulators of immune cell effector function^{63–69}. Thus, with the deletion of HIF-1 α in BMDMs, it is possible that Myc and other transcription factors shift BMDMs toward a primarily mitochondria-dominated metabolism that favors proliferation/cellular maintenance rather than a glycolytic phenotype that is poised for robust inflammatory effector function.

In conclusion, HIF-1 α is not required for TR-AM function under steady-state conditions or for inflammatory effector function, and only hypoxic conditions necessitate HIF-1 α glycolytic reprogramming in TR-AMs to ensure optimal cellular fitness. HIF-1 α functions much differently in BMDMs. HIF-1 α is required for basal glycolytic metabolism and optimal proinflammatory effector function in BMDMs but is dispensable for LPS-induced glycolytic flux. Moreover, the loss of HIF-1 α in BMDMs enhances mitochondrial function potentially in a c-Myc-dependent manner. These data describe a divergent role for HIF-1 α in primary macrophage subsets and may be beneficial in developing therapies for ARDS where TR-AMs function to alleviate disease while infiltrating, nonresident macrophages exacerbate disease.

Limitations of the study

We would like to point out that utilizing an inducible myeloid lineage cell specific HIF-1 α deletion system to delete HIF-1 α from cells is not without controversy. This system may not delete HIF-1 α in 100% of cells upon tamoxifen exposure. Likewise, *Lyz2CreERT2* allele results in *Lyz2* heterozygosity in our cells. However, we show that lysozyme protein expression is largely maintained in our cells (Supplementary Fig. S12). Based on our metabolic findings and the existing literature, we believe that the observed phenotype in our knockout macrophages is a result of HIF-1 α deletion. While BMDMs derived in CSF-1 may not perfectly recapitulate the phenotype of recruited macrophages, we have previously shown that BMDMs and recruited macrophages have similar metabolic phenotypes^{9,12}. Furthermore, while hypoxia is a more physiological activator of HIF-1 α , we chose to use a chemical prolyl hydroxylase inhibitor in attempt to induce HIF-1 α while eliminating the off-target cellular effects associated with low oxygen levels particularly the direct effect of hypoxia on the mitochondria. Our group and others have shown that HIF-independent hypoxic responses have significant impacts on inflammation and metabolic pathways outside of canonical HIF-1 α signaling^{12,70}.

Methods

Animals

All studies in animals were approved by the Institutional Animal Care and Use Committee at the University of Chicago. All experiments were performed in accordance with the relevant guidelines and regulations. The study is reported in accordance with ARRIVE guidelines^{71,72}. Euthanasia was performed by intraperitoneal injection of Euthasol (a sodium pentobarbital-based euthanasia solution) followed by a secondary method including bilateral thoracotomy, and exsanguination. All strains of mice were purchased from The Jackson Laboratory (Bar Harbor, ME). To generate mice with tamoxifen-inducible myeloid lineage cell specific deletion of *Hif1a* (*Hif1a*^{fl/fl}:*LysM-CreERT2*^{+/-}), we crossed *Hif1a*^{fl/fl} mice (B6.129-*Hif1a*^{tm3Rsjol}/J) (Jackson Strain #: 007561) with *LysM-CreERT2*^{+/-} mice (heterozygous for inducible Cre recombinase) (*Lyz2*^{tm1(cre/ERT2)Grnl}/J) (Jackson Strain #: 031674). *Hif1a*^{fl/fl} mice have *loxP* sites flanking exon 2 of the *Hif1a* gene. Exposure to Cre recombinase removes the floxed sequence creating a null allele through the excision of exon 2. Confirmation of Exon 2 deletion was assessed via qPCR (Primer sequences: *Rpl19* (5'-CCGACGAAAGGGTATGCTCA-3', 5'-GACCTTCTTTTTC CCGCAGC-3'), and *Hif1a* exon 2 (5'-AGATCTCGGCGAAGCAAAGA, 5'-ACATTGTGGGGAAGTGGCAA-3'). (Supplementary Fig. S1). We then treated *Hif1a*^{fl/fl}:*LysM-CreERT2*^{+/-} and *Hif1a*^{fl/fl}:*LysM-CreERT2*^{-/-} mice with tamoxifen (80 mg/kg/day) dissolved in corn oil for 5 days to generate *Hif1a*^{-/-} macrophages or tamoxifen-treated control (*Hif1a*^{+/+}) macrophages, respectively.

Primary culture of macrophages

We used well-accepted methods to isolate and culture both macrophage populations as we have previously described^{9,12,42,73}. These methods yield TRAMs at a purity greater than 95%. BMDMs are assumed to be nearly 100% pure as they are bone marrow cells differentiated into macrophages over seven days with M-CSF. To isolate TR-AMs, we euthanized 6–8 week old male mice and performed standard bronchoalveolar lavage via intratracheal instillation of PBS with 0.5 mM EDTA. Following isolation, TR-AMs were counted, plated in RPMI 1640 (ThermoFisher, Cat# 11875119) supplemented with 10% FBS (Gemini, Cat# 100–106) and 1%

penicillin-streptomycin (Gemini, Cat# 400–109), and allowed to adhere to tissue culture plates for one hour prior to experimentation. BMDMs were generated by isolating bone marrow cells from the femur and tibia bones of 6–8 week old *Hif1a*^{-/-} and *Hif1a*^{+/-} mice. Bone marrow cells were differentiated into BMDMs on petri dishes using 40 ng/mL recombinant M-CSF (BioLegend, Cat# 576406) and 1 µg/mL 4-Hydroxytamoxifen (Millipore Sigma, Cat# SML1666) in the same media formulation as TR-AMs. On day seven, after successful differentiation and gene deletion, BMDMs were replated and allowed to adhere to tissue culture plates for two hours prior to experimentation. After adherence, cells were washed and placed with fresh media under experimental conditions. FG-4592, a prolyl hydroxylase inhibitor, was used at a concentration of 25 µM for HIF-1α stabilization. Lyophilized FG-4592 was dissolved in DMSO and diluted 1:2500 in media to achieve a final concentration of 25 µM. DMSO diluted to 1:2500 in media served as untreated control groups. For inflammatory stimulation, LPS was used at a concentration of 20 ng/mL.

Bioenergetic measurements

Glycolytic and mitochondrial respiration rates were measured using the XFe24 Extracellular Flux Analyzer (Agilent, Santa Clara, MA). BMDMs and TR-AMs were seeded at 4.0×10^4 /well onto Seahorse XF24 Cell Culture Microplates. Cells were equilibrated with XF Base media (Agilent, Cat# 103334-100) at 37 °C for 30 min in the absence of CO₂. The glycolytic rate was assessed using the manufacturers' protocol for the Seahorse XF Glycolysis Stress Test followed by sequential injections with glucose (10 mM), oligomycin (1.0 µM), and 2-DG (100 mM). Mitochondrial respiration rate was measured using the Seahorse XF Mito Stress Test according to the manufacturer's protocol followed by sequential injections with oligomycin (1.0 µM), FCCP (1.0 µM for BMDMs and 4.0 µM for TR-AMs), and rotenone/antimycin A (1.0 µM). Assessment of real-time metabolic responses to LPS was performed using the protocol detailed in an application note provided by the Agilent²². In brief, following plating, cells were equilibrated in XF base media supplemented with 10 mM glucose, 2 mM L-glutamine, 1 mM sodium pyruvate (Sigma, Cat# 11360070) and 5 mM HEPES (Sigma, Cat# 15630080), pH 7.4 and incubated at 37 °C without CO₂ for 30 min prior to XF assay. Baseline metabolic rates were measured followed by direct injection of LPS (final concentration: 20 ng/mL). Bioenergetic rates were subsequently measured every three minutes for approximately 5 h in total.

Cell lysis, subcellular fractionalization and Immunoblotting

Whole cell lysates were prepared by scraping cells into lysis buffer containing 25 mM Tris•HCl (pH 7.6), 150 mM NaCl, 1% NP-40, 1% sodium deoxycholate, 0.1% SDS, 0.1% Benzamide, and Halt™ Protease Inhibitor Cocktail (ThermoFisher, Cat# 78430). Samples were centrifuged at 16,000 × g at 4 °C for 5 min to pellet cellular debris. Subcellular fractionalization and lysate preparation were carried out using the NE-PER Nuclear and Cytoplasmic Extraction Reagents (ThermoFisher, Cat# 78833). Lysate protein concentration was determined using the Pierce™ BCA Protein Assay Kit (ThermoFisher, Cat# 23225). Samples were heated to 95 °C for 5 min and equal concentrations of samples (15 µg for whole cell lysates and 5 µg for nuclear fractions) were resolved on Criterion 4–20% gels (Bio-Rad, Cat# 5671093, and 5671094) and transferred to nitrocellulose (Bio-Rad, Cat# 1620167). Primary antibodies used were rabbit anti-HK2 (Cell Signaling, Cat# C64G5, 1:1000), rabbit anti-LDHA (Cell Signaling, Cat# 20125, 1:1000), rabbit anti-PHD2/Egln1 (Cell Signaling, Cat# 4835, 1:1000), rabbit anti-MCT4 (Proteintech, Cat# 22787-1-AP), rabbit anti-Lamin B1 (Proteintech, Cat# 12987-1-AP, 1:1000), rabbit anti-HIF-1α (Cayman Chemical, Cat# 10006421, 1:500), rabbit anti-c-Myc (Abcam, Cat# ab32072), and rabbit anti-α-tubulin (Proteintech, Cat# 11224-1-AP, 1:2,000). Secondary antibodies used were anti-rabbit IgG HRP-linked antibody (Cell Signaling, Cat# 7074, 1:2,500) and anti-mouse IgG HRP-linked antibody (Cell Signaling, Cat# 7076, 1:2,500). Protein expression was visualized using Immobilon ECL Ultra Western HRP Substrate (Millipore Sigma, Cat# WBULS0500) in combination with the BioRad ChemiDoc Touch Imaging system. All immunoblot data were repeated in at least three independent experiments.

Total ETC Immunoblotting

Whole cell lysates were collected and quantified as described in the previous methods section. Samples were heated to 37 °C for 30 min and equal concentrations of samples (15 µg) were resolved on Criterion 12% gels (Bio-Rad, Cat# 5671044) and transferred to PVDF (Bio-Rad, Cat# 1620177). Mitochondrial complex proteins were resolved using mouse anti-OXPHOS Rodent WB Antibody cocktail (Abcam, Cat# ab110413, 1:1000).

SiRNA knockdown

SiRNA knockdown was performed using the Amaxa Mouse Macrophage Nucleofector Kit (Lonza, Cat# VPA-1009). 1.0×10^6 cells/reaction were resuspended in transfection solution with siRNA of interest (Dharmacon, Non-Targeting Control siRNA: D-001810-01; mouse *Hif1a* siRNA: J-040638-06; mouse *Myc* siRNA: J-040813-05). The cell solution was then subjected to electroporation (Lonza Nucleofector 2b Electroporator: Setting Y-001). Cells were plated and allowed to rest for 48 h prior to further experimentation.

Cytokine analysis

Secreted TNFα, IL-6, KC, and IL-1β levels were evaluated in macrophage media using a standard sandwich ELISA (R&D Systems DuoSet ELISA Development System, Cat# DY410, DY406, DY453, and DY401). For IL-1β sample collection, 5 mM ATP was added to macrophage cultures for 30 min following 6 h LPS treatment to activate caspase 1, ensuring proIL-1β cleavage and IL-1β release. Rotenone and Antimycin A concentrations were 20 nM when used in ELISA experiments.

Sulforhodamine B (SRB) colorimetric assay

In vitro cytotoxicity was measured using the SRB assay⁷⁴. Following treatment, cells were fixed in 10% TCA and then stained with SRB dye. Cellular protein-dye complexes were solubilized in 10mM Tris base and the samples were read at OD 510 using a microplate reader. Data was normalized to the untreated, *Hif1a*^{+/+} groups, which were representative of no cellular damage. ETC inhibitor concentrations were as follows: 500nM rotenone, and 500nM antimycin.

Immunofluorescence

Macrophages were plated at 4.0×10^4 cells in 50 μ l of media on chamber slides (ThermoFisher, Cat# 177402PK) to prevent cell dispersion toward the chamber edges. Once adhered, an additional 150 μ l of media containing treatment conditions (Final concentration: 20ng/ml LPS or 25 μ M FG-4592) was added to the chamber slides. After 4 hours, the media was carefully removed with a micropipette (no vacuum suction) and the cells were fixed in 4% paraformaldehyde for 20 min at room temperature (RT). Treatments were handled in this fashion because the macrophages peel off the glass slide with little agitation prior to fixation. Following fixation, cells were permeabilized in blocking solution (0.1% Triton X100, 3% FBS in PBS) for 60 min at RT. Both primary rabbit anti-HIF1 α antibody (Abcam, Cat# ab179483, 1:100) and secondary Goat anti-rabbit CoraLite⁴⁸⁸-Conjugated (Proteintech, Cat# SA00013-2, 1:400) incubations took place overnight at 4°C in a humidifying chamber. Coverslips were then mounted ProLong[™] Glass Antifade Mountant with NucBlue[™] Stain (ThermoFisher, Cat# P36983). Fluorescent images were obtained using the Zeiss Axio Observer 7 Microscope. Images were prepared for publication using QuPath bioimaging software⁷⁵. The same brightness and contrast settings were maintained across all sample images to ensure accurate comparison.

Gas chromatography mass spectrometry (GC-MS) for metabolite measurements

Macrophages were plated at 2.5×10^5 on 24-well plates for metabolite extraction. Following treatment, cells were washed with ice-cold blood bank saline (ThermoFisher, Cat# 23-293-184) and cells were scrapped into 600 μ l of 80% methanol with 1 μ g Norvaline/600 μ l. The metabolite samples were vortexed and centrifuged at 16,000 \times g at 4 °C for 10 min to precipitate insoluble material. 400 μ l of the liquid sample was then dried under nitrogen gas for approximately 2 h until no liquid remained. Samples then underwent derivatization, a process involving the addition of chemical modifiers to the metabolites for a more sensitive and accurate identification. First, samples were incubated in 16 μ l Methoxamine (MOX) Reagent (ThermoFisher, Cat# TS45950) for 1 h at 37°C. Samples were then incubated for 1 h at 60°C following the addition of 20 μ l of tert-Butyldimethylsilyl (tBDMs) (Sigma, Cat# 394882). Derivatized samples were analyzed with an 8890 gas chromatograph with an HP-5MS column (Agilent) coupled with a 5977B Mass Selective Detector mass spectrometer (Agilent). Helium was used as the carrier gas at a flow rate of 1.2 ml/min. One microliter of each sample was injected in split mode (1:4 for BMDMs; 1:2 for TR-AMs) at 280 °C. After injection, the GC oven was held at 100 °C for 1 min and increased to 300 °C at 3.5 °C/min. The oven was then ramped to 320 °C at 20 °C/min and held for 5 minutes. The MS system was operated under electron impact ionization at 70 eV and the MS source was operated at 230 °C and quadrupole at 150 °C. The detector was used in scanning mode, and the scanned ion range was 100–650 m/z . Peak ion chromatograms for metabolites of interest were extracted at their specific m/z with Mass Hunter Quantitative Analysis software (Agilent Technologies). Ions used for quantification of metabolite levels were as follows: Pyruvate m/z 174, Lactate m/z 233, Citrate m/z 591, Itaconate m/z 303, Succinate m/z 289, Fumarate m/z 287, Malate m/z 419, Aspartate m/z 390. For each sample, total ion counts for all metabolites were normalized internally to norvaline. All samples were then normalized to controls (HIF1 α ^{fl/fl}; no treatment) for quantification and statistical comparison.

RNA-sequencing

Total RNA was extracted from cells using the GenElute[™] Mammalian Total RNA Miniprep Kit (Millipore Sigma Cat#: RTN350). RNA quality was evaluated with a Bioanalyzer (Agilent), ensuring RIN values greater than 8.5. RNA was then submitted for sequencing at the University of Chicago Genomics Core Facility using the Illumina NovaSEQ6000 sequencer (paired-end). FASTQ files were generated and assessed for quality per base sequence using FastQC. RNA-seq data is accessible via GEO (GSE279117). RNA-seq reads were pseudoaligned with Kallisto v.0.44.0 at the Center for Research Informatics on the Randi high-performance computing cluster at the University of Chicago⁷⁶. The Kallisto index was created with default settings using GENCODE (GRCm39), and quantification was performed in its default mode. Gene abundance calculations were conducted with the tximport R package v.1.18.0. Differential expression analysis was carried out using the edgeR R package, which involved read count filtering, normalization, dispersion estimation, and the identification of differentially expressed genes⁷⁷. The library (Rtsne) was used for dimensionality reduction and visualization of variance and relationships between individual samples. Genes were considered significantly differentially expressed if they had an FDR-adjusted p-value ≤ 0.05 and a fold change (FC) greater than 2. Results were visualized with heatmaps generated from Z-score normalized expression data using the pheatmap package. Gene Ontology - Biological Process enrichment analyses plots were created using R cluster profiler package “enrichGO” function⁷⁸. Genes sets used in heatmap analysis (CHEA Hif1- α target, Glycolytic and oxidative phosphorylation, c-Myc target) genes were obtained from Harmonizome, a multi-omics data integration platform⁷⁹. Transcription factor (TF) target gene interactions gene regulatory network enrichment analysis was done with R DoRothEA package using mouse regulons²⁵.

Statistics

The data were analyzed in Prism 10 (GraphPad Software Inc.). All data are shown as mean \pm SD unless otherwise specified. ANOVA was used for statistical analyses of data sets containing more than two groups, and Bonferroni's *post hoc* test was used to explore individual differences. Statistical significance was defined as $P < 0.05$.

Data availability

The raw source data for RNA-seq are accessible via GEO (GSE279117). <https://www.ncbi.nlm.nih.gov/geo/que ry/acc.cgi?acc=GSE279117>.

Received: 17 October 2024; Accepted: 25 March 2025

Published online: 04 April 2025

References

- Krawczyk, C. M. et al. Toll-like receptor-induced changes in glycolytic metabolism regulate dendritic cell activation. *Blood* **115**, 4742–4749. <https://doi.org/10.1182/blood-2009-10-249540> (2010).
- Ip, W. K. E., Hoshi, N., Shouval, D. S., Snapper, S. & Medzhitov, R. Anti-inflammatory effect of IL-10 mediated by metabolic reprogramming of macrophages. *Science* **356**, 513–519. <https://doi.org/10.1126/science.aal3535> (2017).
- Freemerman, A. J. et al. Metabolic reprogramming of macrophages: Glucose transporter 1 (GLUT1)-mediated glucose metabolism drives a Proinflammatory phenotype. *J. Biol. Chem.* **289**, 7884–7896. <https://doi.org/10.1074/jbc.M113.522037> (2014).
- Frauwirth, K. A. et al. The CD28 signaling pathway regulates glucose metabolism. *Immunity* **16**, 769–777. [https://doi.org/10.1016/S1074-7613\(02\)00323-0](https://doi.org/10.1016/S1074-7613(02)00323-0) (2002).
- Borregaard, N. & Herlin, T. Energy metabolism of human neutrophils during phagocytosis. *J. Clin. Invest.* **70**, 550–557. <https://doi.org/10.1172/JCI110647> (1982).
- Caputa, G., Castoldi, A. & Pearce, E. J. Metabolic adaptations of tissue-resident immune cells. *Nat. Immunol.* **20**, 793–801. <https://doi.org/10.1038/s41590-019-0407-0> (2019).
- Gautier, E. L. et al. Gene-expression profiles and transcriptional regulatory pathways that underlie the identity and diversity of mouse tissue macrophages. *Nat. Immunol.* **13**, 1118–1128. <https://doi.org/10.1038/ni.2419> (2012).
- Lavin, Y. et al. Tissue-Resident macrophage enhancer landscapes are shaped by the local microenvironment. *Cell* **159**, 1312–1326. <https://doi.org/10.1016/j.cell.2014.11.018> (2014).
- Woods, P. S. et al. Tissue-Resident alveolar macrophages do not rely on Glycolysis for LPS-induced inflammation. *Am. J. Respir. Cell. Mol. Biol.* **62**, 243–255. <https://doi.org/10.1165/rcmb.2019-0244OC> (2020).
- Svedberg, F. R. et al. The lung environment controls alveolar macrophage metabolism and responsiveness in type 2 inflammation. *Nat. Immunol.* **20**, 571–580. <https://doi.org/10.1038/s41590-019-0352-y> (2019).
- Baker, E. H. & Baines, D. L. Airway glucose homeostasis: A new target in the prevention and treatment of pulmonary infection. *Chest* **153**, 507–514. <https://doi.org/10.1016/j.chest.2017.05.031> (2018).
- Woods, P. S. et al. HIF-1 α induces glycolytic reprogramming in tissue-resident alveolar macrophages to promote cell survival during acute lung injury. *Elife* <https://doi.org/10.7554/eLife.77457> (2022).
- van de Laar, L. et al. Yolk sac macrophages, fetal liver, and adult monocytes can colonize an empty niche and develop into functional Tissue-Resident macrophages. *Immunity* **44**, 755–768. <https://doi.org/10.1016/j.immuni.2016.02.017> (2016).
- Semenza, G. L. Hypoxia-inducible factors in physiology and medicine. *Cell* **148**, 399–408. <https://doi.org/10.1016/j.cell.2012.01.021> (2012).
- Cramer, T. et al. HIF-1 α is essential for myeloid cell-mediated inflammation. *Cell* **112**, 645–657. [https://doi.org/10.1016/S0092-8674\(03\)00154-5](https://doi.org/10.1016/S0092-8674(03)00154-5) (2003).
- Palsson-McDermott, E. M. et al. Pyruvate kinase M2 regulates Hif-1 α activity and IL-1 β induction and is a critical determinant of the Warburg effect in LPS-activated macrophages. *Cell. Metab.* **21**, 65–80. <https://doi.org/10.1016/j.cmet.2014.12.005> (2015).
- Peyssonnaud, C. et al. HIF-1 α expression regulates the bactericidal capacity of phagocytes. *J. Clin. Invest.* **115**, 1806–1815. <https://doi.org/10.1172/JCI23865> (2005).
- Tannahill, G. M. et al. Succinate is an inflammatory signal that induces IL-1 β through HIF-1 α . *Nature* **496**, 238–242. <https://doi.org/10.1038/nature11986> (2013).
- Izquierdo, H. M. et al. Von Hippel-Lindau protein is required for optimal alveolar macrophage terminal differentiation, Self-Renewal, and function. *Cell. Rep.* **24**, 1738–1746. <https://doi.org/10.1016/j.celrep.2018.07.034> (2018).
- Mookerjee, S. A., Goncalves, R. L. S., Gerencser, A. A., Nicholls, D. G. & Brand, M. D. The contributions of respiration and Glycolysis to extracellular acid production. *Biochim. Et Biophys. Acta (BBA) - Bioenergetics*. **1847**, 171–181. <https://doi.org/10.1016/j.bbabi.2014.10.005> (2015).
- Corcoran, S. E. & O'Neill, L. A. J. HIF1 α and metabolic reprogramming in inflammation. *J. Clin. Invest.* **126**, 3699–3707. <https://doi.org/10.1172/JCI84431> (2016).
- Kam, Y. & Dranka, S. P. BP. Real time discrimination of inflammatory macrophage activation using agile seahorse XF technology (white paper). (2017).
- Wang, F. et al. Interferon Gamma Induces Reversible Metabolic Reprogramming of M1 Macrophages to Sustain Cell Viability and Pro-Inflammatory Activity. *eBioMedicine* **30**, 303–316. <https://doi.org/10.1016/j.ebiom.2018.02.009> (2018).
- van Riggelen, J., Yetil, A. & Felsher, D. W. MYC as a regulator of ribosome biogenesis and protein synthesis. *Nat. Rev. Cancer*. **10**, 301–309. <https://doi.org/10.1038/nrc2819> (2010).
- Holland, C. H., Szalai, B. & Saez-Rodriguez, J. Transfer of regulatory knowledge from human to mouse for functional genomics analysis. *Biochim. Et Biophys. Acta (BBA) - Gene Regul. Mech.* **1863**, 194431. <https://doi.org/10.1016/j.bbagr.2019.194431> (2020).
- Gordan, J. D., Thompson, C. B. & Simon, M. C. HIF and c-Myc: Sibling rivals for control of cancer cell metabolism and proliferation. *Cancer Cell*. **12**, 108–113. <https://doi.org/10.1016/j.ccr.2007.07.006> (2007).
- Ghoneim, H. E., Thomas, P. G. & McCullers, J. A. Depletion of alveolar macrophages during influenza infection facilitates bacterial superinfections. *J. Immunol.* **191**, 1250–1259. <https://doi.org/10.4049/jimmunol.1300014> (2013).
- Grant, R. A. et al. Circuits between infected macrophages and T cells in SARS-CoV-2 pneumonia. *Nature* **590**, 635–641. <https://doi.org/10.1038/s41586-020-03148-w> (2021).
- Liao, M. et al. Single-cell landscape of Bronchoalveolar immune cells in patients with COVID-19. *Nat. Med.* **26**, 842–844. <https://doi.org/10.1038/s41591-020-0901-9> (2020).
- Dawson, T. C., Beck, M. A., Kuziel, W. A., Henderson, F. & Maeda, N. Contrasting effects of CCR5 and CCR2 deficiency in the pulmonary inflammatory response to influenza A virus. *Am. J. Pathol.* **156**, 1951–1959. [https://doi.org/10.1016/S0002-9440\(10\)65068-7](https://doi.org/10.1016/S0002-9440(10)65068-7) (2000).
- Lin, K. L., Sweeney, S., Kang, B. D., Ramsburg, E. & Gunn, M. D. CCR2-Antagonist prophylaxis reduces pulmonary immune pathology and markedly improves survival during influenza infection. *J. Immunol.* **186**, 508–515. <https://doi.org/10.4049/jimmunol.1001002> (2011).

32. Goetzman, E. S. & Prochownik, E. V. The role for Myc in coordinating glycolysis, oxidative phosphorylation, glutaminolysis, and fatty acid metabolism in normal and neoplastic tissues. *Front. Endocrinol. (Lausanne)*. **9**, 129. <https://doi.org/10.3389/fendo.2018.00129> (2018).
33. Li, L. et al. Transcriptional regulation of the Warburg effect in cancer by SIX1. *Cancer Cell*. **33**, 368–385e367. <https://doi.org/10.1016/j.ccell.2018.01.010> (2018).
34. Ma, H. et al. The transcription factor Foxp1 regulates aerobic Glycolysis in adipocytes and myocytes. *J. Biol. Chem.* **299**, 104795. <https://doi.org/10.1016/j.jbc.2023.104795> (2023).
35. Shim, H. et al. c-Myc transactivation of LDH-A: implications for tumor metabolism and growth. *Proc. Natl. Acad. Sci. U S A*. **94**, 6658–6663. <https://doi.org/10.1073/pnas.94.13.6658> (1997).
36. Ruiz-García, A. et al. Cooperation of adenosine with macrophage Toll-4 receptor agonists leads to increased glycolytic flux through the enhanced expression of PFKFB3 gene. *J. Biol. Chem.* **286**, 19247–19258. <https://doi.org/10.1074/jbc.M110.190298> (2011).
37. Xie, M. et al. PKM2-dependent Glycolysis promotes NLRP3 and AIM2 inflammasome activation. *Nat. Commun.* **7**, 13280. <https://doi.org/10.1038/ncomms13280> (2016).
38. Rius, J. et al. NF- κ B links innate immunity to the hypoxic response through transcriptional regulation of HIF-1 α . *Nature* **453**, 807–811. <https://doi.org/10.1038/nature06905> (2008).
39. Zhang, W. et al. Evidence that hypoxia-inducible factor-1 (HIF-1) mediates transcriptional activation of interleukin-1 β (IL-1 β) in astrocyte cultures. *J. Neuroimmunol.* **174**, 63–73. <https://doi.org/10.1016/j.jneuroim.2006.01.014> (2006).
40. Martínez-Reyes, I. & Chandel, N. S. Mitochondrial TCA cycle metabolites control physiology and disease. *Nat. Commun.* **11**, 102. <https://doi.org/10.1038/s41467-019-13668-3> (2020).
41. Mills, E. L. et al. Itaconate is an anti-inflammatory metabolite that activates Nrf2 via alkylation of KEAP1. *Nature* **556**, 113–117. <https://doi.org/10.1038/nature25986> (2018).
42. Sun, K. A. et al. Endogenous Itaconate is not required for particulate matter-induced NRF2 expression or inflammatory response. *Elife* <https://doi.org/10.7554/eLife.54877> (2020).
43. Swain, A. et al. Comparative evaluation of Itaconate and its derivatives reveals divergent inflammasome and type I interferon regulation in macrophages. *Nat. Metabolism*. **2**, 594–602. <https://doi.org/10.1038/s42255-020-0210-0> (2020).
44. Divakaruni, A. S. et al. Etomoxir inhibits macrophage polarization by disrupting coa homeostasis. *Cell. Metab.* **28**, 490–503e497. <https://doi.org/10.1016/j.cmet.2018.06.001> (2018).
45. Lauterbach, M. A. et al. Toll-like receptor signaling rewires macrophage metabolism and promotes histone acetylation via ATP-Citrate lyase. *Immunity* **51**, 997–1011e1017. <https://doi.org/10.1016/j.immuni.2019.11.009> (2019).
46. Wellen, K. E. et al. ATP-citrate lyase links cellular metabolism to histone acetylation. *Science* **324**, 1076–1080. <https://doi.org/10.1126/science.1164097> (2009).
47. Vats, D. et al. Oxidative metabolism and PGC-1 β attenuate macrophage-mediated inflammation. *Cell Metabol.* **4**, 13–24. <https://doi.org/10.1016/j.cmet.2006.05.011> (2006).
48. Zhu, B. et al. Inhibition of the mitochondrial pyruvate carrier simultaneously mitigates hyperinflammation and hyperglycemia in COVID-19. *Sci. Immunol.* **8**, eadf0348. <https://doi.org/10.1126/sciimmunol.adf0348> (2023).
49. Zhu, B. et al. Uncoupling of macrophage inflammation from self-renewal modulates host recovery from respiratory viral infection. *Immunity* **54**, 1200–1218e1209. <https://doi.org/10.1016/j.immuni.2021.04.001> (2021).
50. Akagawa, K. S., Kamoshita, K. & Tokunaga, T. Effects of granulocyte-macrophage colony-stimulating factor and colony-stimulating factor-1 on the proliferation and differentiation of murine alveolar macrophages. *J. Immunol.* **141**, 3383–3390. <https://doi.org/10.4049/jimmunol.141.10.3383> (1988).
51. Chen, B. D., Mueller, M. & Chou, T. H. Role of granulocyte/macrophage colony-stimulating factor in the regulation of murine alveolar macrophage proliferation and differentiation. *J. Immunol.* **141**, 139–144. <https://doi.org/10.4049/jimmunol.141.1.139> (1988).
52. Hussell, T. & Bell, T. J. Alveolar macrophages: Plasticity in a tissue-specific context. *Nat. Rev. Immunol.* **14**, 81–93. <https://doi.org/10.1038/nri3600> (2014).
53. Courvan, E. M. C. & Parker, R. R. Hypoxia and inflammation induce synergistic transcriptome turnover in macrophages. *Cell. Rep.* **43**, 114452. <https://doi.org/10.1016/j.celrep.2024.114452> (2024).
54. Carmeliet, P. et al. Role of HIF-1 α in hypoxia-mediated apoptosis, cell proliferation and tumour angiogenesis. *Nature* **394**, 485–490. <https://doi.org/10.1038/28867> (1998).
55. Koshiji, M. et al. HIF-1 α induces cell cycle arrest by functionally counteracting Myc. *EMBO J.* **23**, 1949–1956. <https://doi.org/10.1038/sj.emboj.7600196> (2004). <https://doi.org/10.1038/sj.emboj.7600481> (2004).
56. Liu, L. et al. Proinflammatory signal suppresses proliferation and shifts macrophage metabolism from Myc-dependent to HIF1 α -dependent. *Proceedings of the National Academy of Sciences* **113**, 1564–1569 (2016). <https://doi.org/10.1073/pnas.1518000113>.
57. Attwooll, C., Denchi, E. L. & Helin, K. The E2F family: specific functions and overlapping interests. *EMBO J.* **23**, 4709–4716. <https://doi.org/10.1038/sj.emboj.7600481> (2004).
58. Jensen-Cody, C. W. et al. LEF-1 controls cell cycle progression in airway basal cells to regulate proliferation and differentiation. *Stem Cells*. **39**, 1221–1235. <https://doi.org/10.1002/stem.3386> (2021).
59. Yasui, K., Okamoto, H., Arii, S. & Inazawa, J. Association of over-expressed TFDPI with progression of hepatocellular carcinomas. *J. Hum. Genet.* **48**, 609–613. <https://doi.org/10.1007/s10038-003-0086-3> (2003).
60. Liao, M. & Wang, J. Tcf12 balances the reconstitution and differentiation capacity of hematopoietic stem cell. *Blood Sci.* **3**, 14–19. <https://doi.org/10.1097/bs9.0000000000000059> (2021).
61. Rodriguez-Colman, M. J., Dansen, T. B. & Burgering, B. M. T. FOXO transcription factors as mediators of stress adaptation. *Nat. Rev. Mol. Cell Biol.* **25**, 46–64. <https://doi.org/10.1038/s41580-023-00649-0> (2024).
62. Yamamoto, K. et al. A novel function of Onecl1 protein as a negative regulator of MafA gene expression**. *J. Biol. Chem.* **288**, 21648–21658. <https://doi.org/10.1074/jbc.M113.481424> (2013).
63. Ai, K. et al. Methyl-CpG-binding domain protein 2 contributes to renal fibrosis through promoting polarized M1 macrophages. *Cell Death Dis.* **13**, 125. <https://doi.org/10.1038/s41419-022-04577-3> (2022).
64. Gopal, R. et al. STAT2 signaling regulates macrophage phenotype during influenza and bacterial Super-Infection. *Front. Immunol.* **9**, 2151. <https://doi.org/10.3389/fimmu.2018.02151> (2018).
65. Hedvat, C. V., Yao, J., Sokolic, R. A. & Nimer, S. D. Myeloid ELFI-like factor is a potent activator of Interleukin-8 expression in hematopoietic cells**. *J. Biol. Chem.* **279**, 6395–6400. <https://doi.org/10.1074/jbc.M307524200> (2004).
66. Huang, Q. et al. Spi-B promotes the recruitment of Tumor-Associated macrophages via enhancing CCL4 expression in lung cancer. *Front. Oncol.* **11**, 659131. <https://doi.org/10.3389/fonc.2021.659131> (2021).
67. Ohl, K. et al. The transcription factor CREM drives an inflammatory phenotype of T cells in oligoarticular juvenile idiopathic arthritis. *Pediatr. Rheumatol.* **16**, 39. <https://doi.org/10.1186/s12969-018-0253-x> (2018).
68. Xu, H. et al. Notch-RBP-J signaling regulates the transcription factor IRF8 to promote inflammatory macrophage polarization. *Nat. Immunol.* **13**, 642–650. <https://doi.org/10.1038/ni.2304> (2012).
69. Wang, J. et al. Transcription factor T-bet regulates inflammatory arthritis through its function in dendritic cells. *J. Clin. Invest.* **116**, 414–421. <https://doi.org/10.1172/jci26631> (2006).

70. Arsham, A. M., Howell, J. J. & Simon, M. C. A novel Hypoxia-inducible Factor-independent hypoxic response regulating mammalian target of Rapamycin and its targets*. *J. Biol. Chem.* **278**, 29655–29660. <https://doi.org/10.1074/jbc.M212770200> (2003).
71. du Percie, N. et al. The ARRIVE guidelines 2.0: updated guidelines for reporting animal research. *PLoS Biol.* **18**, e3000410. <https://doi.org/10.1371/journal.pbio.3000410> (2020).
72. Kilkenney, C., Browne, W. J., Cuthill, I. C., Emerson, M. & Altman, D. G. Improving bioscience research reporting: the ARRIVE guidelines for reporting animal research. *PLoS Biol.* **8**, e1000412. <https://doi.org/10.1371/journal.pbio.1000412> (2010).
73. Zhang, X., Goncalves, R. & Mosser, D. M. The isolation and characterization of murine macrophages. *Curr Protoc Immunol Chap.* **14**, 14 11 11–14 11 14 (2008). <https://doi.org/10.1002/0471142735.im1401s83>
74. Vichai, V. & Kirtikara, K. Sulforhodamine B colorimetric assay for cytotoxicity screening. *Nat. Protoc.* **1**, 1112–1116. <https://doi.org/10.1038/nprot.2006.179> (2006).
75. Bankhead, P. et al. QuPath: open source software for digital pathology image analysis. *Sci. Rep.* **7**, 16878. <https://doi.org/10.1038/s41598-017-17204-5> (2017).
76. Bray, N. L., Pimentel, H., Melsted, P. & Pachter, L. Near-optimal probabilistic RNA-seq quantification. *Nat. Biotechnol.* **34**, 525–527. <https://doi.org/10.1038/nbt.3519> (2016).
77. Robinson, M. D., McCarthy, D. J. & Smyth, G. K. EdgeR: a bioconductor package for differential expression analysis of digital gene expression data. *Bioinformatics* **26**, 139–140. <https://doi.org/10.1093/bioinformatics/btp616> (2010).
78. Yu, G., Wang, L. G., Han, Y. & He, Q. Y. ClusterProfiler: An R package for comparing biological themes among gene clusters. *Omics* **16**, 284–287. <https://doi.org/10.1089/omi.2011.0118> (2012).
79. Rouillard, A. D. et al. The harmonizome: a collection of processed datasets gathered to serve and mine knowledge about genes and proteins. *Database (Oxford)* (2016). (2016) <https://doi.org/10.1093/database/baw100>

Acknowledgements

This work was supported by funding from the Department of Defense grant HT9425-24-1-0138 (GMM), and from NIH grants R01HL151680 (RBH), F32HL167569 (ORS), R01ES015024 (GMM), and T32HL007605 (GMM).

Author contributions

P.S.W., R.B.H., G.M.M. conceptualized and designed the study. P.S.W., R.C.A., A.Y.M., K.A.S., O.R.S., K.W.D.S., Y.F., B.H. conducted the experiments. P.S.W., A.Y.M., K.A.S., R.B.H., G.M.M. performed data analysis. R.C.A. and K.W.D.S. analyzed the sequencing data. P.S.W., R.B.H., G.M.M. wrote the initial draft, with all other authors providing comments. P.S.W., R.C.A., R.B.H., G.M.M. edited the manuscript. All authors read and approved the manuscript.

Declarations

Competing interests

The authors declare no competing interests.

Additional information

Supplementary Information The online version contains supplementary material available at <https://doi.org/10.1038/s41598-025-95962-3>.

Correspondence and requests for materials should be addressed to G.M.M.

Reprints and permissions information is available at www.nature.com/reprints.

Publisher's note Springer Nature remains neutral with regard to jurisdictional claims in published maps and institutional affiliations.

Open Access This article is licensed under a Creative Commons Attribution-NonCommercial-NoDerivatives 4.0 International License, which permits any non-commercial use, sharing, distribution and reproduction in any medium or format, as long as you give appropriate credit to the original author(s) and the source, provide a link to the Creative Commons licence, and indicate if you modified the licensed material. You do not have permission under this licence to share adapted material derived from this article or parts of it. The images or other third party material in this article are included in the article's Creative Commons licence, unless indicated otherwise in a credit line to the material. If material is not included in the article's Creative Commons licence and your intended use is not permitted by statutory regulation or exceeds the permitted use, you will need to obtain permission directly from the copyright holder. To view a copy of this licence, visit <http://creativecommons.org/licenses/by-nc-nd/4.0/>.

© The Author(s) 2025